remote sensing

MDPI

Article

Theoretical Calculations of Directional Scattering Intensities of Small Nonspherical Ice Crystals: Implications for Forward Scattering Probes

Seonghyeon Jang [1], Jeonggyu Kim [1], Greg M. McFarquhar [2], Sungmin Park [1], Seoung Soo Lee [3,4], Chang Hoon Jung [5], Sang Seo Park [6], Joo Wan Cha [7], Kyoungmi Lee [7] and Junshik Um [1,8,*]

1 Department of Atmospheric Sciences, Division of Earth Environmental System, BK21 School of Earth and Environment Systems, Pusan National University, Busan 46241, Korea; ball4590@pusan.ac.kr (S.J.); wjdrb501@pusan.ac.kr (J.K.); rkgkth@pusan.ac.kr (S.P.)
2 Cooperative Institute for Severe and High Impact Weather Research and Operations, School of Meteorology, University of Oklahoma, Norman, OK 73072, USA; mcfarq@ou.edu
3 Earth System Science Interdisciplinary Center, University of Maryland, College Park, MD 20740, USA; cumulss@gmail.com
4 Research Center for Climate Sciences, Pusan National University, Busan 46241, Korea
5 Department of Health Management, Kyungin Women's University, Incheon 21041, Korea; jch@kiwu.ac.kr
6 Department of Urban and Environmental Engineering, Ulsan National Institute of Science and Technology, Ulsan 44919, Korea; sangseopark@unist.ac.kr
7 Research Applications Department, National Institute of Meteorological Sciences, Seogwipo 63568, Korea; jwcha@korea.kr (J.W.C.); leekm80@korea.kr (K.L.)
8 Department of Atmospheric Sciences, Pusan National University, Busan 46241, Korea
* Correspondence: jjunum@pusan.ac.kr; Tel.: +82-51-510-2171

Citation: Jang, S.; Kim, J.; McFarquhar, G.M.; Park, S.; Lee, S.S.; Jung, C.H.; Park, S.S.; Cha, J.W.; Lee, K.; Um, J. Theoretical Calculations of Directional Scattering Intensities of Small Nonspherical Ice Crystals: Implications for Forward Scattering Probes. *Remote Sens.* **2022**, *14*, 2795. https://doi.org/10.3390/rs14122795

Academic Editor: Anthony J. Baran

Received: 10 May 2022
Accepted: 7 June 2022
Published: 10 June 2022

Abstract: In situ aircraft measurements of the sizes and concentrations of liquid cloud droplets and ice crystals with maximum dimensions (D_{max}) less than ~50 μm have been measured mainly using forward scattering probes over the past half century. The operating principle of forward scattering probes is that the measured intensity of light scattered by a cloud particle at specific forward scattering angles can be related to the size of that particle assuming the shape and thermodynamic phase of the target are known. Current forward-scattering probes assume spherical liquid cloud droplets and use the Lorenz–Mie theory to convert the scattered light to particle size. Uncertainties in sizing ice crystals using forward scattering probes are unavoidable since the single-scattering properties of ice crystals differ from those of spherical liquid cloud droplets and because their shapes can vary. In this study, directional scattering intensities of four different aspect ratios (ARs = 0.25, 0.50, 1.00, and 2.00) of hexagonal ice crystals with random orientations and of spherical liquid cloud droplets were calculated using the discrete dipole approximation (i.e., ADDA) and Lorenz–Mie code, respectively, to quantify the errors in sizing small ice crystals and cloud droplets using current forward scattering probes and to determine the ranges of optimal scattering angles that would be used in future forward scattering probes. The calculations showed that current forward scattering probes have average 5.0% and 17.4% errors in sizing liquid cloud droplets in the forward (4–12°) and backward (168–176°) direction, respectively. For measurements of hexagonal ice crystals, average sizing errors were 42.1% (23.9%) in the forward (backward) direction and depended on the ARs of hexagonal ice crystals, which are larger than those for liquid cloud droplets. A newly developed size conversion table based on the calculated single-scattering properties of hexagonal ice crystals using the ADDA reduced the sizing errors for the hexagonal ice crystals down to 14.2% (21.9%) in the forward (backward) direction. This study is a purely theoretical examination of the operating principle of forward scattering probes and there are several limitations, such as assumed hexagonal ice crystals with smooth surfaces and random orientations.

Keywords: forward scattering probe; nonspherical ice crystal; sizing error; optimal scattering angle; Lorenz–Mie theory; discrete dipole approximation

1. Introduction

Clouds are divided into liquid, mixed, and ice-phase according to their thermodynamic phase. Unlike liquid clouds, which are composed of spherical liquid cloud droplets, ice clouds are composed of ice crystals with various shapes and sizes [1–3]. Spherical liquid cloud droplets and nonspherical ice crystals coexist in mixed-phase clouds. It is difficult to calculate the microphysical and radiative properties of mixed- and ice-phase clouds because ice crystals have broad size ranges and various non-spherical shapes. However, the distribution of sizes and shapes (i.e., habits) of cloud particles is fundamental information and the most important knowledge to characterize the microphysical and radiative properties of clouds.

Because clouds exist at relatively high altitudes, aircraft have exclusively been used for in situ cloud observations. In general, cloud particles with maximum dimension (D_{max}) smaller than 50 μm have been measured using directional scattering intensity-based probes mounted on aircraft, such as forward scattering probes. Two-dimensional optical array probes, such as two-dimensional cloud (2DC) and precipitation (2DP) imaging probes [4], cloud imaging (CIP) and precipitation imaging (PIP) probes [5], the 2D stereo (2DS) probe and the high-volume precipitation spectrometer (HVPS) [6,7], have determined the size and shape of larger cloud particles by continuously saving the shadows of cloud particles on photodiodes when cloud particles pass over a series of multiple diode arrays [8–11]. The operating principle of forward scattering probes is totally different. When a cloud particle passes the sample area of a forward scattering probe, a laser beam is scattered by the cloud particle and the directional intensity of scattered light is measured at specific forward angles, which can be related to the size of cloud particles based on the Lorenz–Mie theory [8,10,11]. However, current conversion tables are valid only for spherical shape and known composition (i.e., refractive index) of a target for a given wavelength of incident light. Thus, typical forward scattering probes do not provide shapes of cloud particles, but sizes and concentrations of cloud particles.

As all measurement instruments have unavoidable intrinsic uncertainties, forward scattering probes also have uncertainty (e.g., uncertainties related to small sample volume). Since the main products of forward scattering probes are the sizes and concentrations of cloud particles, the measurement uncertainties can be categorized for each [8,12]. The uncertainties related to particle sizing are mainly due to Mie ambiguity (also known as Mie oscillation or resonance), particle shape (i.e., spherical or nonspherical), and particle coincidence. The relationship between the size of a cloud particle and the intensity of scattered light at specific scattering (i.e., collecting) angles, which is formulated by the Lorenz–Mie theory, is not monotonic but oscillating [8,11,13–17]. For example, theoretical calculations have shown that the errors in sizing are as large as 100% for spherical particles with D_{max} < 10 μm, less than 10% for spherical particles with 10 < D_{max} < 30 μm, and further increasing for spherical particles with D_{max} > 30 μm [18]. Small variations of collecting angles due to imperfect optical mounting exist even between versions of the same probe, which invokes additional uncertainties in sizing cloud particles [18–20]. The shape (e.g., spherical vs. nonspherical) of a particle is a crucial factor that determines its single-scattering properties [21]. Thus, the measurement uncertainties of forward scattering probes depend heavily on the existence of spherical cloud droplets and/or correctly determining the shapes of nonspherical ice crystals. However, the impacts of nonspherical ice crystals on the measurement accuracy of forward scattering probes have not been well established, which is one of the foci of this study.

Multiple particles can be observed in the sample volume of a forward scattering probe at the same time, which causes uncertainties in both particle sizing and counting, which is known as the coincidence problem [18,22–27]. Splashing of liquid cloud droplets and shattering of large ice crystals on the tips or shrouds of cloud probes may also impact particle concentrations [28–34]. Numerous efforts have been made to develop calibration methods and processing techniques to reduce the measurement uncertainties of forward scattering probes [5,12–14,18,20,22,23,26,29,35–38].

Forward scattering probes or on-axis scattering spectrometers [8] were originally developed to observe small spherical liquid cloud droplets and have been used over 50 years since the development of the Particle Measuring Systems (PMS) FSSP 100 [39,40]. Several other forward scattering probes, such as the cloud aerosol spectrometer (CAS) [5], cloud droplet probe (CDP) [14], fast CDP (FCDP), fast FSSP (FFSSP), cloud and aerosol spectrometer with polarization (CAS-POL) [41], cloud particle spectrometer with polarization detection (CPSPD) [42], have also been developed based on an almost identical working principle (i.e., Lorenz–Mie theory) with an assumption of the presence of spherical liquid cloud droplets.

The use of forward scattering probes for observations of ice crystals causes several problems. First, the refractive index of ice crystals differs from that of liquid cloud droplets. More importantly, there are large discrepancies between the single-scattering properties of nonspherical small ice crystals and those of spherical liquid cloud droplets. Although the degradation of measurement accuracy of forward scattering probes has been reported in the presence of ice crystals [28,29,43,44], forward scattering probes have been used to measure the sizes and concentrations of ice crystals with D_{max} < 50 μm without quantifying the corresponding uncertainties.

The *T*-matrix [45] has been used for calculating the single-scattering properties of axial-symmetric cylinders and spheroids representing shapes of natural ice crystals. It was reported that the errors in sizing of nonspherical ice crystals measured by forward scattering probes were up to 20% [46,47] with its use. The assumption of axial-symmetric shape was solely due to the limitation of the *T*-matrix method. However, a cloud chamber experiment showed that at least 60% of generated small ice crystals were hexagonal columns [48]. Since a hexagonal lattice structure is the basic structure of an ice crystal, a hexagonal column or plate is the fundamental shape of small ice crystals [3]. Subsequent studies [8,17] examined the impacts of nonspherical ice crystals on the measurements of forward scattering probes by using realistic hexagonal shapes of ice crystals and the discrete dipole approximation to calculate the corresponding single-scattering properties. It was shown that the errors in sizing of nonspherical ice crystals using forward scattering probes were at least 13% (26%) for forward (backward) collecting angles and could be up to 120% (132%). However, these studies had limited calculations and can be improved significantly.

Theoretical calculations of the directional scattering intensities of small spherical liquid cloud droplets and nonspherical ice crystals are performed here to quantify the impact of nonsphericity on the measurement accuracy of forward scattering probes, to examine whether the ranges of forward and backward scattering angles that are currently used in forward scattering probes are suitable to measure sizes of small ice crystals and liquid cloud droplets, and to determine the optimal scattering angles in the forward and backward directions that minimize sizing errors for future versions of forward scattering probes. All other uncertainties existing in forward scattering probes [8,18] except the sizing errors caused by large variabilities of single-scattering properties of small cloud particles due to different shapes, sizes, and thermodynamic phase, are not considered in this study. Thus, this study is a purely theoretical examination of the operating principle of forward scattering probes. Section 2 describes the methods and uncertainties in determining the size of a cloud particle measured by a forward scattering probe. In Section 3, the methodology to calculate the single-scattering properties of small ice crystals and to quantify sizing errors for forward scattering probes is explained. The quantified errors in sizing nonspherical ice crystals and spherical liquid cloud droplets using forward scattering probes are explained in Section 4. The determined optimal scattering angles of forward scattering probes are shown in Section 5, followed by summarizing and discussing the most important findings of this study in Section 6.

2. The Operating Principle of Forward Scattering Probes to Determine a Size of a Cloud Particle

When a cloud particle passes through the laser beam of a forward scattering probe, light is scattered by the cloud particle and the distribution of the directional intensities of scattered light depend on the wavelength of the laser beam and the size, shape, and composition (i.e., refractive index) of the cloud particle. Part of the scattered light that is collected at certain angles in forward and/or backward directions is directed to two detectors called the sizer and qualifier. When a cloud particle lies within the depth of field of the qualifier (i.e., in-focus), the detected signal of the qualifier exceeds that of the sizer and the particle is counted [42]. The intensity of scattered light detected by the sizer without an optical mask is converted to the equivalent optical diameter (i.e., particle size) based on a pre-calculated conversion table that relates the differential scattering cross-section to the size of a particle. Assumptions of spherical (i.e., shape) liquid (i.e., refractive index) cloud droplets are applied to generate the conversion table for a given wavelength of laser using the Lorenz–Mie theory. Table 1 summarizes the wavelengths of laser and light collection angles used in forward scattering probes (i.e., on-axis scattering spectrometers).

Table 1. Specification of forward scattering probes (i.e., on-axis scattering spectrometers).

Probe Name	Measurement Range (μm)	Wavelength (nm)	Light Collection Angles (°)
FSSP	2–50	633	3–13°
CDP	2–50	658	4–12°
CAS	0.5–50	658	4–12°, 168–176°
FFSSP	1–50	632	4–12°
FCDP	1–50	785	4–12°
CAS-POL	0.6–50	680	4–12°, 168–176°
CPSPD	0.65–30	658	13–47°, 133–167°

Besides the on-axis scattering spectrometer type forward scattering probes shown in Table 1, several other types of probes have been used to measure the sizes and concentrations of small cloud particles. A small ice detector (SID) was developed to distinguish ice and liquid phase of cloud particles based on the measurements of high-resolution distributions of two-dimensional light scattering patterns collected over wide scattering angle ranges (e.g., 9–20° or 7–25°). A family of SID models, SID-1 [49], SID-2 [25], and SID-3 [50], have been thus used to measure sizes and shapes of cloud particles with ~2 < D_{max} < 140 μm. A novel holographic technique probe (e.g., HALOHolo) [51] has an effective pixel size less than 3 μm and provides sizes and shapes of cloud particles with ~6 < D_{max} < 5000 μm. A cloud particle imager has a 2.3 μm pixel resolution (actual resolution of ~5 μm) and measures the sizes and shapes of cloud particles [52]. A particle habit imaging and polar scattering probe provide the dual images and directional intensities of scattered light of cloud particles whose sizes are as small as ~5 μm [53]. A particle volume monitor that is classified as a laser-diffraction particle-sizing instrument measures higher moments of cloud particle size distribution [54,55]. Although such instruments measure small cloud particles, the most common in situ probes measuring small particles are still the on-axis scattering spectrometer type forward scattering probes (e.g., CAS, CDP, and FSSP). Thus, this study focuses on the sizing errors of on-axis scattering spectrometers.

Figure 1 shows example scattering-phase functions (P_{11}) of spherical liquid cloud droplets with maximum dimensions D_{max} (i.e., diameters) of 3 and 12 μm determined using a Lorenz–Mie code [56] at a wavelength λ = 0.55 μm. Forward scattering angles of 4–12° and backward scattering angles of 168–176° that are used for the light collection angles of forward scattering probes (e.g., CAS) are shaded. More complex features in P_{11} are shown for larger cloud droplets (i.e., D_{max} = 12 μm). Based on the intensities of scattered light at

these angles, the differential scattering cross-sections of cloud droplets are calculated and shown in Figure 2. The relationship between the calculated differential scattering cross-section and particle size shows a highly nonlinear feature, especially for the smaller sizes and at the backward scattering angles. For a given (i.e., measured) differential cross-section, multiple particle sizes are possible due to the Mie ambiguity that is mainly caused by an interaction between diffracted and transmitted light. The effect of Mie ambiguity is higher at forward scattering angles compared with that at backward scattering angles. An effect of resonance also contributes to Mie ambiguity although its effect is much smaller than that of the interaction. It was shown that the impact of Mie ambiguity was especially large for small cloud droplets (D_{max} < 10 μm) [8] as also shown in Figure 2.

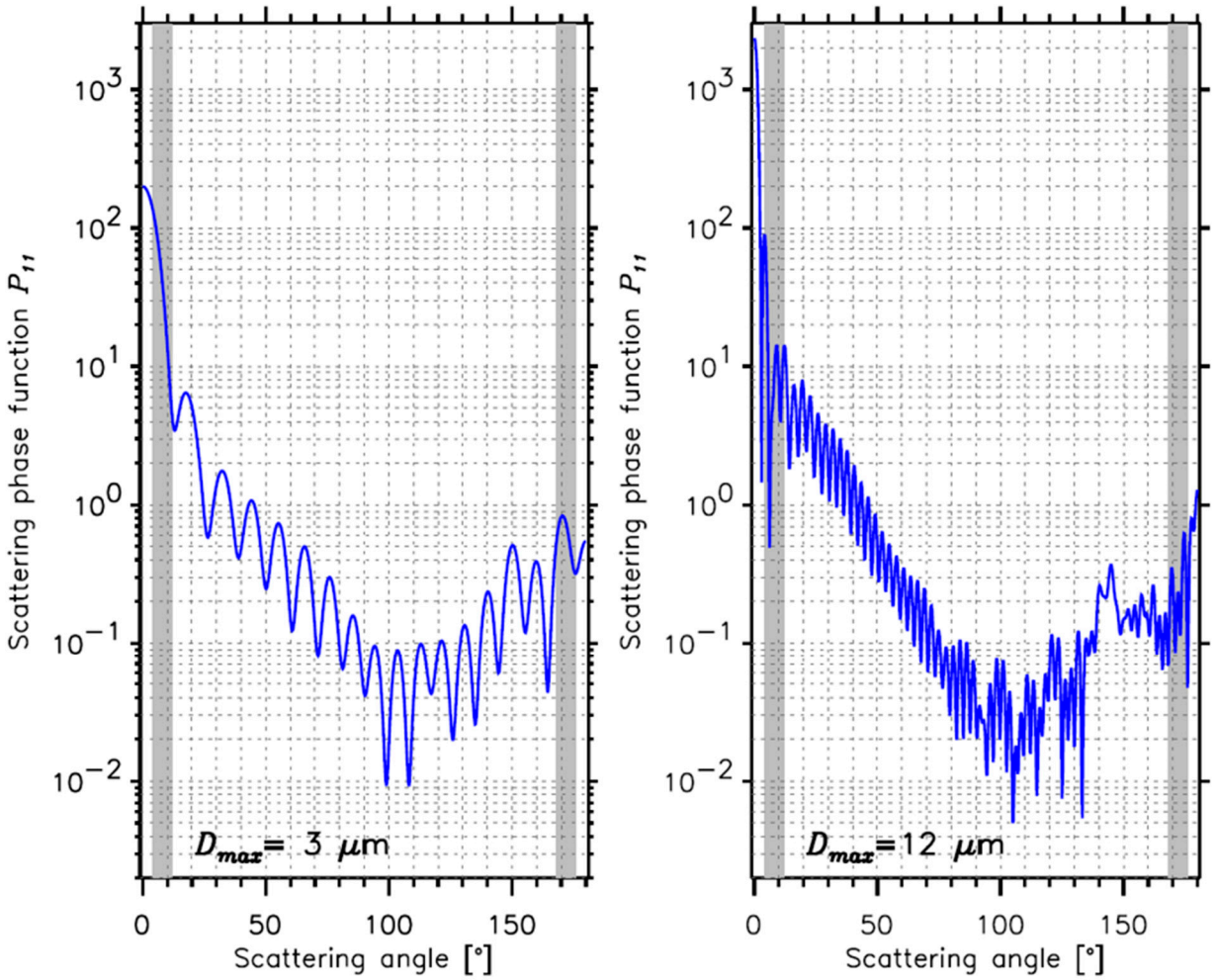

Figure 1. Calculated scattering phase function (P_{11}) of spherical liquid cloud droplets with maximum dimensions D_{max} = 3 μm (**left**) and D_{max} = 12 μm (**right**) using a Lorenz–Mie code at a wavelength λ = 0.55 μm. The ranges of light collection angles in forward (4–12°) and backward (168–176°) directions are shaded in each panel.

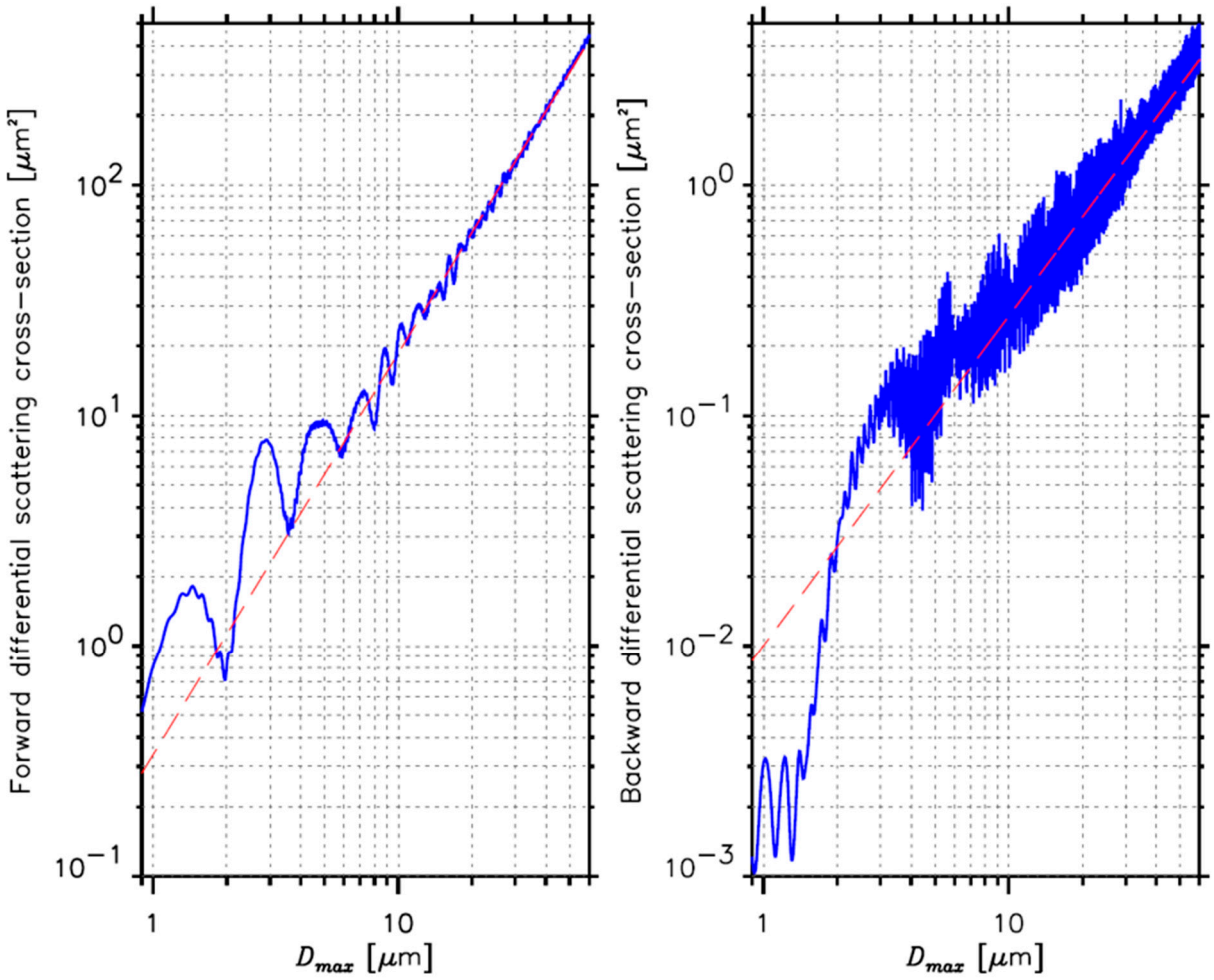

Figure 2. Calculated differential scattering cross-sections (blue) of liquid cloud droplets as a function of maximum dimension in forward (4–12°, **left**) and backward (168–176°, **right**) directions. A best-fit line (red) is embedded in each panel.

Several methods have been proposed to minimize the errors in particle sizing due to the Mie ambiguity. For example, relocating or combining size bins [14,15,57,58] and smoothing of differential scattering cross-sections by applying a running average [58] have been suggested. In this study, the errors in particle sizing were determined using two different methods. One is to use the exact calculations of differential scattering cross-sections (i.e., blue lines in Figure 2) and the other uses best-fit calculations (i.e., red lines in Figure 2) which is similar to the smoothing method [58]. For this purpose, calculations of single-scattering properties of spherical and nonspherical cloud particles with D_{max} < 50 μm were calculated as explained in Section 3.

3. Methodology

3.1. Idealized Models Representing Shapes of Small Cloud Particles

Identifying the shapes of natural ice crystals whose sizes fall within the measurement range (i.e., ~1–50 μm) of forward scattering probes has large uncertainties even using state-of-the-art cloud imaging probes mainly due to insufficient resolution and diffraction [2,59]. Thus, several idealized models representing shapes of small ice crystals have been proposed. For example, a simple spherical shape [60], a Chebyshev particle [61], a droxtal [62], a Gaussian random sphere [63], and a budding Bucky ball [2] have been used to calculate the single-scattering properties of small ice crystals, which show strong dependence on the assumed idealized model. The calculated single-scattering properties of small ice crystals far differ from those of spherical liquid cloud droplets and, thus, such properties

are required to determine the impact of nonspherical ice crystals on the measurement accuracy of forward scattering probes.

Since a hexagonal lattice structure is a fundamental structure of ordinary ice crystal Ih [64], shapes of hexagonal columns are inherent shapes of natural small ice crystals that are diffusionally growing. One exception might be the quasi-spherical shapes of frozen droplets formed by homogeneous freezing that were found near the strong convective cores of anvil clouds [65–68]. In this study, hexagonal columns were used to represent shapes of small ice crystals and the corresponding single-scattering properties calculated. A hexagonal column is characterized by a length (L), width (W), and aspect ratio ($AR = L/W$) as shown in Figure 3. Since the observed natural hexagonal ice crystals showed wide ranges of ARs [69] four different ARs of 0.25, 0.50, 1.00, and 2.00 were used in this study. A maximum dimension (D_{max}) defined as $\sqrt{(L^2 + W^2)}$ was referred to as the size of hexagonal ice crystal. Table 2 summarizes dimensional information of hexagonal ice crystals used for the calculations of single-scattering properties in this study.

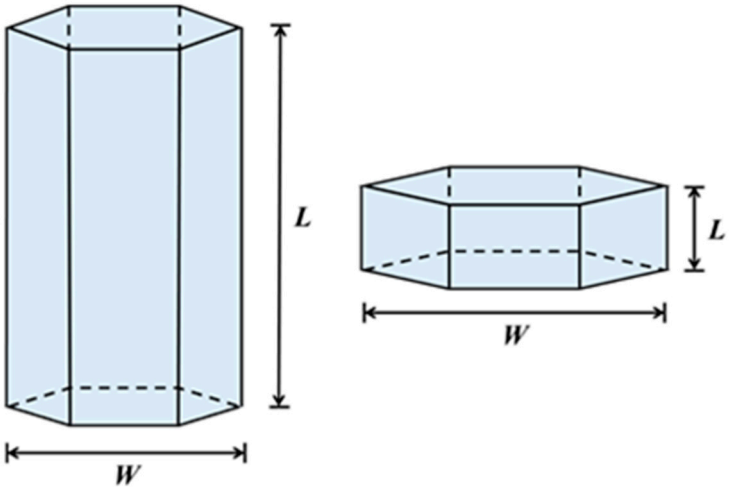

Figure 3. Shapes of hexagonal columns with length (L) and width (W). Aspect ratio (AR) is defined as $AR = L/W$. The long column (**left**) has a higher AR, while the thin plate (**right**) has a smaller AR.

Table 2. Dimensional information of hexagonal ice crystals for a given aspect ratio (AR) used in this study. The L, W, and D_{max} is the length, width, and maximum dimension of a hexagonal ice crystal, respectively. A size parameter (χ_{Dmax}) is defined as $\chi_{Dmax} = \pi D_{max}/\lambda$.

	***AR* = 0.25**	***AR* = 0.50**	***AR* = 1.00**	***AR* = 2.00**
L (μm)	0.0625–7.0	0.125–10.0	0.25–20.00	0.50–32.0
W (μm)	0.25–28.0	0.25–20.0	0.25–20.0	0.25–16.0
D_{max}	0.26–28.86	0.28–22.36	0.35–28.28	0.56–35.78
χ_{Dmax}	1.47–164.86	1.60–127.72	2.02–161.56	3.19–204.36

3.2. Single-Scattering Properties and Differential Scattering Cross-Section of Small Cloud Particles

For liquid cloud droplets a spherical shape was assumed and the corresponding single-scattering properties (i.e., P_{11}) of spheres with D_{max} between 0.01 and 800 μm (0.01 μm intervals) were calculated using a Lorenz–Mie code [56] at λ = 0.55 μm. Such a large size range is required to determine the sizing errors as shown in Section 5. At λ = 0.55 μm, the refractive index of liquid water is $1.333 + i1.960 \times 10^{-9}$.

The single-scattering properties of four different *AR*s of hexagonal columns with D_{max} < 50 μm (Table 2) were calculated at λ = 0.55 μm where the refractive index of ice crystal is $1.311 + i1.960 \times 10^{-9}$ [70]. A numerically exact method, the ADDA (formerly coined as Amsterdam discrete dipole approximation but now officially ADDA) [71], was used for the calculations of single-scattering properties of hexagonal columns. For all ADDA calculations a conservative criterion of $A < 0.5$ was used, where A is a constant for the validity criterion of $kd\,|\,m\,| < A$, which is required to mimic the geometry of the target with high accuracy in single-scattering calculations [3,71]. Here, k, d, m is the wavenumber of incident light, diameter of dipole, and complex refractive index of a target, respectively. The single-scattering properties of various shapes and sizes of ice crystals using an another numerically exact method, the invariant imbedding T-matrix method, were compared against those using the ADDA and they showed agreement [72]. For all ADDA simulations hexagonal columns were assumed to have random orientations that were represented by a two-dimensional Halton sequence [3,17,73,74]. The required criteria for the accurate ADDA calculations and the orientation average using the quasi-Monte Carlo method (i.e., two-dimensional Halton sequence) used in this study are found in previous studies [3,73].

Based on the calculated P_{11} of small cloud particles, a differential scattering cross-section C_{sca} for a forward scattering probe would measure is calculated as:

$$C_{sca,\theta} = \frac{1}{k^2} \int_0^{2\pi} \int_{\theta_1}^{\theta_2} P_{11} \sin(\theta) d\theta d\phi \tag{1}$$

where θ and ϕ is a scattering angle and azimuth angle, respectively. A pair of scattering angles (θ_1 and θ_2) is selected according to the light collection angles of a forward scattering probe (Table 1). To determine the accuracy of current forward scattering probes (i.e., Section 4), $\theta_1 = 4^\circ$ and $\theta_2 = 12^\circ$ ($\theta_1 = 168^\circ$ and $\theta_2 = 176^\circ$) were used for the forward (backward) direction, which are the light collection angles of CAS. To find the optimal scattering angles (i.e., Section 5), the pair of scattering angles (θ_1 and θ_2) was varied using intervals of 1°, 2°, 4°, 6°, or 8° between 0° and 180° with a 1° increment.

3.3. Quantification of Sizing Errors

This study quantified percentile sizing errors as:

$$\text{Sizing error } (\%) = \left(\frac{D_{determined} - D_{actual}}{D_{actual}} \right) \times 100\ \% \tag{2}$$

Here, D_{actual} is the actual size (i.e., D_{max}) of a spherical cloud droplet or a nonspherical ice crystal that would be measured. The $D_{determined}$ is the determined D_{max} (i.e., reference value) of a spherical cloud droplet or a nonspherical ice crystal calculated using a Lorenz–Mie code or ADDA, respectively. For the calculations of $D_{determined}$, several combinations of thermodynamic phases and shapes of spherical cloud droplets or nonspherical hexagonal ice crystals were used (see Table 3). All calculations of sizing errors were repeated using an exact and best-fit comparison as explained at the end of Section 2.

Table 3. Configurations to determine sizing errors and the determined sizing errors in Section 4. The average ± standard deviation (maximum) of sizing errors determined using an exact comparison is shown, while those determined using a best-fit comparison are in the square brackets.

Target (Measured Particle, D_{actual})	Pre-Calculation of Cloud Particle		Section	Determined Average ± Standard Deviation (Maximum) Sizing Errors (%)			
	Assumed Phase	Assumed Shape		Forward (4–12°)		Backward (168–176°)	
Spherical liquid cloud droplet	Liquid	Sphere	Section 4.1	5.0 ± 9.7 (121.9) [6.9 ± 16.1 (113.7)]		17.4 ± 12.8 (229.2) [14.6 ± 17.9 (128.7)]	
Hexagonal ice crystal	Liquid	Sphere	Section 4.2.1	*AR* = 0.25	44.2 ± 10.1 (91.3) [45.5 ± 12.8 (77.5)]	*AR* = 0.25	20.6 ± 16.1 (74.8) [20.1 ± 24.3 (90.4)]
				AR = 0.50	40.2 ± 10.1 (58.8) [41.6 ± 9.7 (52.8)]	*AR* = 0.50	15.5 ± 9.0 (66.5) [17.8 ± 15.4 (82.6)]
				AR = 1.00	43.0 ± 11.7 (59.3) [42.9 ± 13.6 (53.8)]	*AR* = 1.00	39.7 ± 10.1 (70.8) [50.6 ± 18.2 (80.4)]
				AR = 2.00	41.1 ± 15.3 (55.4) [40.3 ± 16.3 (55.0)]	*AR* = 2.00	19.6 ± 18.2 (67.9) [21.2 ± 25.0 (91.3)]
	Ice	Sphere	Section 4.2.2	*AR* = 0.25	45.6 ± 10.6 (88.3) [46.6 ± 12.8 (75.1)]	*AR* = 0.25	16.2 ± 14.6 (74.4) [18.0 ± 22.9 (88.7)]
				AR = 0.50	41.6 ± 10.7 (60.3) [42.8 ± 10.2 (52.4)]	*AR* = 0.50	26.7 ± 7.6 (65.9) [31.8 ± 12.4 (79.5)]
				AR = 1.00	44.8 ± 11.2 (62.0) [44.0 ± 14.1 (55.2)]	*AR* = 1.00	58.6 ± 19.4 (98.6) [71.1 ± 25.8 (98.2)]
				AR = 2.00	43.3 ± 14.2 (56.7) [41.3 ± 16.8 (56.3)]	*AR* = 2.00	24.5 ± 11.3 (66.5) [27.9 ± 19.2 (89.8)]
	Ice	Hexagonal column (All *AR*s)	Section 4.2.3	*AR* = 0.25	15.7 ± 14.4 (106.7) [8.3 ± 14.8 (89.1)]	*AR* = 0.25	18.7 ± 3.9 (46.6) [19.3 ± 9.8 (73.7)]
				AR = 0.50	14.3 ± 10.1 (103.3) [7.8 ± 6.2 (70.7)]	*AR* = 0.50	19.3 ± 7.4 (74.3) [13.8 ± 3.9 (58.0)]
				AR = 1.00	12.0 ± 8.5 (69.1) [7.2 ± 10.5 (76.0)]	*AR* = 1.00	33.5 ± 8.6 (86.7) [29.0 ± 2.7 (83.5)]
				AR = 2.00	14.7 ± 10.2 (82.5) [11.4 ± 13.9 (90.1)]	*AR* = 2.00	15.9 ± 3.4 (37.5) [16.3 ± 9.5 (75.4)]
		Hexagonal column (*AR* = 1.0)		*AR* = 1.00	5.6 ± 8.8 (64.9) [13.2 ± 17.7 (70.5)]	*AR* = 1.00	0.0 ± 0.0 (0.0) [8.2 ± 13.2 (53.5)]

4. Sizing Errors Determined for Current Forward Scattering Probes

Figures 4 and 5 show the calculated forward (4–12°) and backward (168–176°) scattering cross-sections of hexagonal ice crystals (red) and spherical liquid cloud droplets (blue), respectively. Four different *AR*s of hexagonal ice crystals are shown, while the scattering cross-sections of spherical liquid cloud droplets calculated using Lorenz–Mie code do not vary with *AR* since *AR* = 1.00 for spherical particles. The scattering cross-sections of hexagonal ice crystals and spherical liquid cloud droplets depend nonlinearly on particle size for D_{max} < ~10 μm in the forward direction. Particles with D_{max} > ~10 μm show a dependence on particle size closer to linear. For larger hexagonal ice crystals whose sizes are beyond the calculation limits of ADDA, the corresponding scattering cross-sections were extrapolated using the ADDA calculations (D_{max} > 10 μm) and are shown with the red broken lines. Thus, some degree of uncertainty may exist for the extrapolated scattering cross-sections. Based on the calculations shown in Figures 4 and 5, the sizing errors using current forward-scattering probes were determined using several combinations of thermodynamic phases and shapes of cloud particles, which are summarized in Table 3.

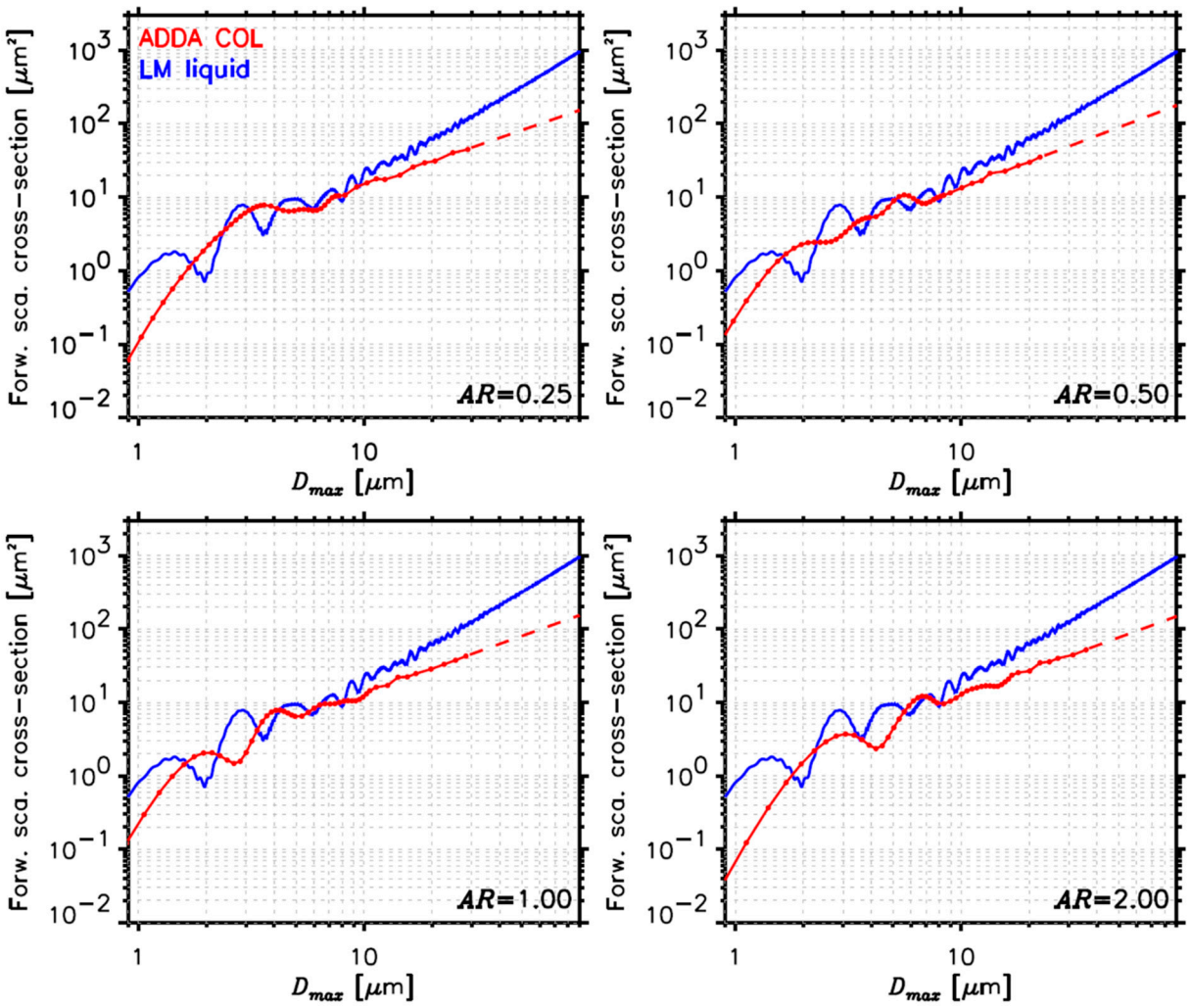

Figure 4. Calculated forward (4–12°) scattering cross-sections of hexagonal ice crystals (red) and spherical liquid cloud droplets (blue) as functions of maximum dimensions of hexagonal ice crystals and spherical liquid cloud droplets using the ADDA and Lorenz–Mie code, respectively, for four different aspect ratios of AR = 0.25, 0.50, 1.00, and 2.00. The extrapolated scattering cross-sections of hexagonal ice crystals are shown with red broken lines.

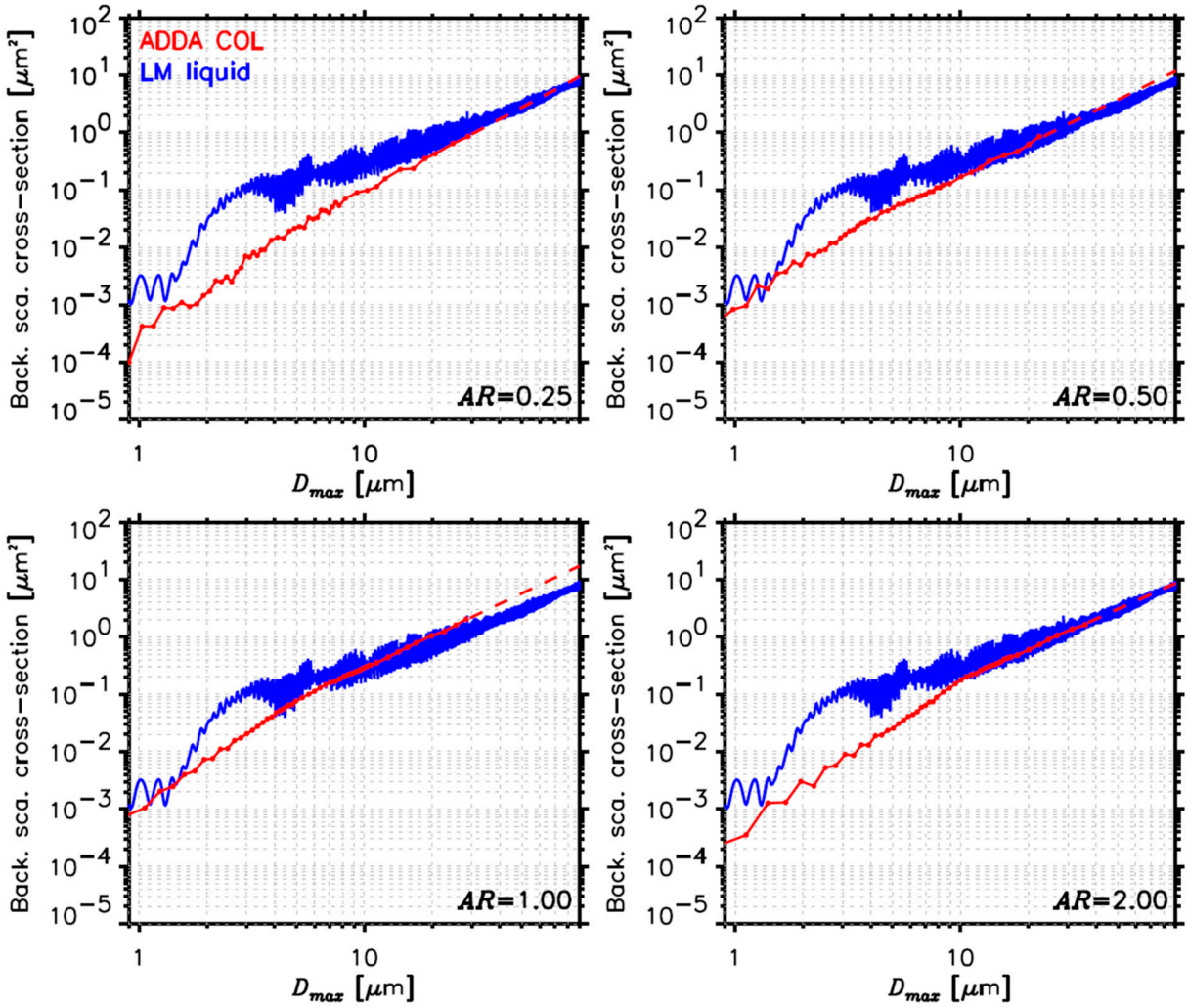

Figure 5. The same as Figure 4, except for backward (168–176°) scattering cross-sections.

4.1. Measurements of Spherical Liquid Cloud Droplets

The first case considered is the common case that a current forward scattering probe (i.e., CAS) measures liquid cloud droplets (i.e., target) whose sizes are determined using the exact calculations (i.e., blue lines in Figures 2, 4 and 5) of the forward and backward scattering cross-sections of spherical liquid cloud droplets using a Lorenz–Mie code. Figure 6 shows the sizing errors of spherical liquid cloud droplets in the forward (4–12°, left) and backward (168–176°, right) directions. For a given size of the measured cloud droplet, multiple determined particle sizes are possible mainly due to the Mie ambiguity. The minimum and maximum sizing errors for a measured particle are the lower and upper boundary of the orange shaded area that encloses all possible sizing errors. The blue lines indicate the average of all sizing errors for a given size of a measured particle. A positive (negative) value of blue line means that the determined size of cloud droplet is overestimated (underestimated). Frequently, the overestimated and underestimated sizing errors for a given size of a particle are compensated for each other and, thus, the blue lines do not represent the averaged sizing errors well. Alternatively, the black lines represent an average of the absolute values of all sizing errors for a given size of a particle. The average and standard deviation of black line across all D_{max} are embedded in each panel.

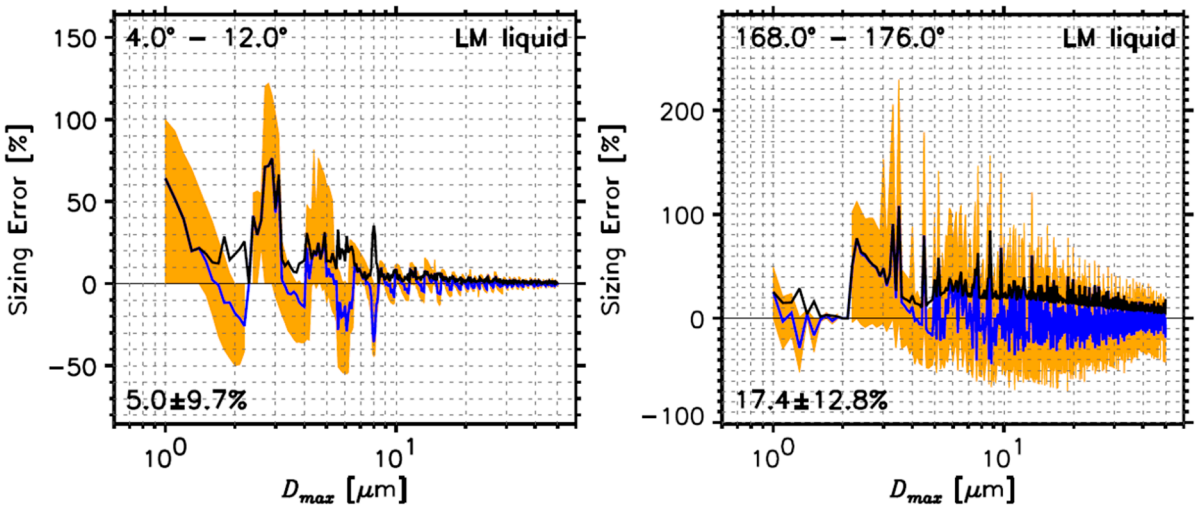

Figure 6. Determined sizing errors of spherical liquid cloud droplets at forward (4–12°, **left**) and backward (168–176°, **right**) scattering angles. The sizing errors are calculated using an exact comparison between the measured D_{max} of liquid cloud droplets and those determined by a Lorenz–Mie code assuming spherical liquid cloud droplets (LM liquid). The minimum and maximum sizing errors are the lower and upper boundary of the orange shaded area where the sizing errors of all possible selections exist. The blue lines indicate the averaged sizing errors of all possible selections for a given size of the sphere, while the black lines are the average of the absolute values of sizing errors of all possible selections. The average and standard deviation of the black line across all sizes are also embedded in each panel.

To summarize Figure 6, it is shown that the current forward scattering probe (i.e., CAS) has 5.0 ± 9.7% (121.9%) of average ± standard deviation (maximum) errors in sizing spherical liquid cloud droplets at forward scattering angles (4–12°), and 17.4 ± 12.8% (229.2%) at backward scattering angles (168–176°). The sizing errors in the forward direction are smaller than those in the backward direction. It is also shown that the larger sizing errors are found for particles smaller than ~10 μm and the errors decrease with particle size.

The calculations of sizing errors were repeated using a best-fit comparison that uses the best-fit lines (i.e., red broken lines in Figure 2) of Lorenz–Mie calculations, instead of the exact calculation. The best-fit comparison was developed to test whether a simple best-fit technique can reduce sizing errors. It provides a singular determined sizing error for a given size of a measured particle and, thus, there is no orange shading area in Figure 7. The determined average ± standard deviation (maximum) in sizing errors at forward scattering angles are 6.9 ± 16.1% (113.7%) and 14.6 ± 17.9% (128.7%) at forward and backward scattering angles, respectively (see Figure 7 and Table 3). Although the best-fit comparison reduces the maximum sizing error compared to the exact comparison, the determined average and standard deviation of sizing errors are increased. Thus, the simple best-fit technique does not improve the sizing errors compared with the exact calculations.

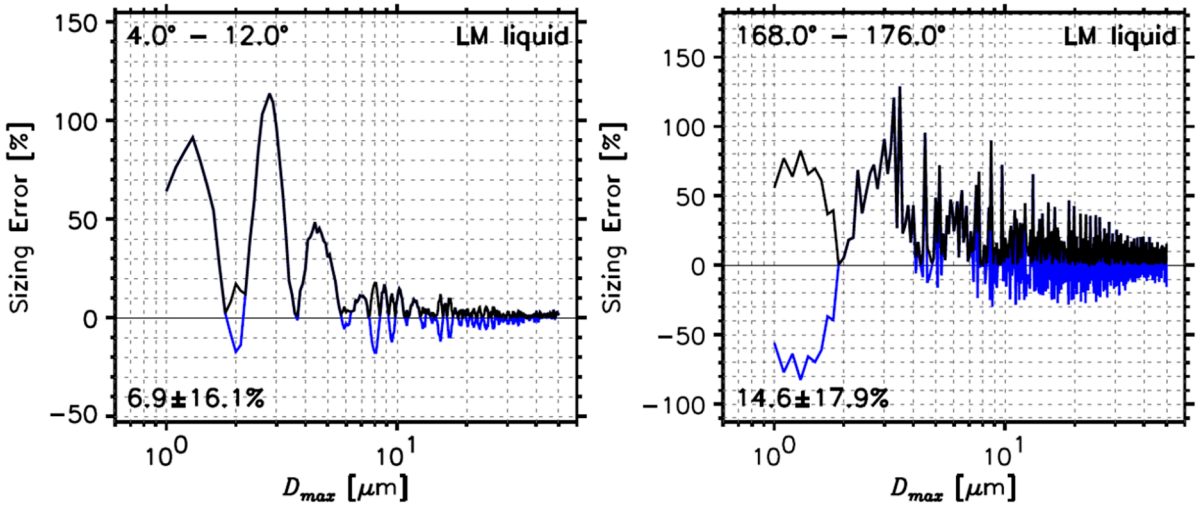

Figure 7. The same as Figure 6, but for a best-fit comparison.

4.2. Measurements of Hexagonal Ice Crystals

4.2.1. Determined Sizing Errors Using Spherical Liquid Cloud Droplets

The second case considered is also a common case that a current forward scattering probe (i.e., CAS) measures hexagonal ice crystals whose sizes are determined using the exact calculations (i.e., blue lines in Figures 2, 4 and 5) of forward and backward scattering cross-sections of spherical liquid cloud droplets using a Lorenz–Mie code. In this case, the phase (i.e., ice) and shape (i.e., hexagonal column) of the measured cloud particle differ from those (i.e., liquid and sphere) assumed in the calculations of a Lorenz–Mie code for a forward scattering probe.

Figure 8 and Table 3 show the sizing errors of hexagonal ice crystals in the forward and backward directions. For each direction four different *AR*s of hexagonal ice crystals are shown. The average ± standard deviations (maximum) of sizing errors are 44.2 ± 10.1% (91.3%), 40.2 ± 10.1% (58.8%), 43.0 ± 11.7% (59.3%), and 41.1 ± 15.3% (55.4%) for AR = 0.25, 0.50, 1.00, and 2.00, respectively, in the forward direction. The sizing errors in the backward direction are, in general, smaller than those in the forward direction and they are 20.6 ± 16.1% (74.8%), 15.5 ± 9.0% (66.5%), 39.7 ± 10.1% (70.8%), and 19.6 ± 18.2% (67.9%). The sizing errors in the forward and backward directions are due to the impacts of different phases and shapes of cloud particles compared with those assumed in a forward scattering probe. In contrast to the measurements of spherical liquid cloud droplets (i.e., Section 4.1), the average sizing errors in the forward direction are larger than those in the backward direction for hexagonal ice crystals. It is revealed that the sizing errors increase with ice crystals with D_{max} > ~8 μm in the forward direction, which is important that there are larger sizing errors for larger ice crystals. Table 3 shows that computations using the best-fit comparison do not improve the results (figures are not shown).

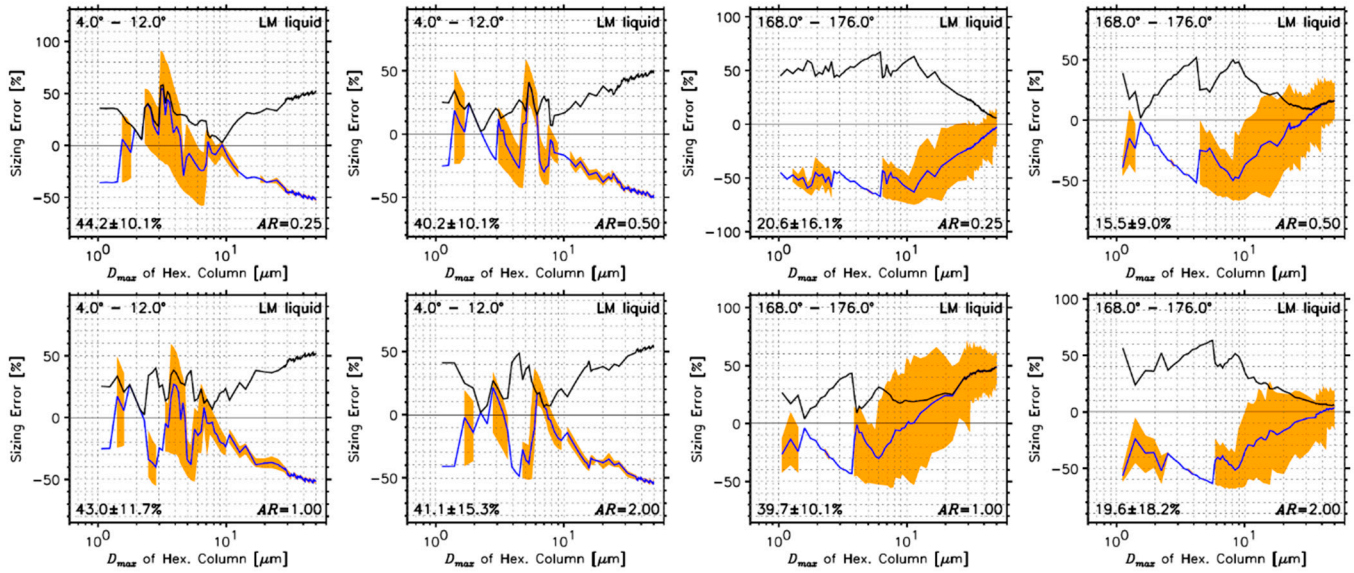

Figure 8. Determined sizing errors of hexagonal ice crystals in forward (4–12°, **left two columns**) and backward (168–176°, **right two columns**) directions. The sizing errors are calculated using an exact comparison between the measured D_{max} of hexagonal ice crystals and those calculated by a Lorenz–Mie code assuming spherical liquid cloud droplets (LM liquid). Each panel represents a different aspect ratio of hexagonal ice crystal. The color scheme is the same as Figure 6.

4.2.2. Determined Sizing Errors Using Spherical Ice Crystals

The third case considered is the uncommon case that a current forward scattering probe (i.e., CAS) measures hexagonal ice crystals whose sizes are determined using the exact calculations of forward and backward scattering cross-sections of spherical ice cloud droplets using a Lorenz–Mie code. To exclude the impact of phase, spherical ice cloud droplets are assumed and, thus, any impact found here is due to the impact of shape.

The determined sizing errors of hexagonal ice crystals in the forward and backward directions are shown in Figure 9 and Table 3. The average ± standard deviations (maximum) of the sizing errors are 45.6 ± 10.6% (88.3%), 41.6 ± 10.7% (60.3%), 44.8 ± 11.2% (62.0%), and 43.3 ± 14.2% (56.7%) for AR = 0.25, 0.50, 1.00, and 2.00, respectively, in the forward direction. The sizing errors in the backward direction are, in general, smaller than those in the forward direction, and are 16.2 ± 14.6% (74.4%), 26.7 ± 7.6% (65.9%), 58.6 ± 19.4% (98.6%), and 24.5 ± 11.3% (66.5%). Replacing spherical liquid cloud droplets with spherical ice cloud droplets does not improve the sizing errors. Thus, the impact of the shape of an ice crystal is larger than that of the phase for measurements of forward scattering probes. Table 3 shows that computations using the best-fit comparison do not improve the results (figures are not shown).

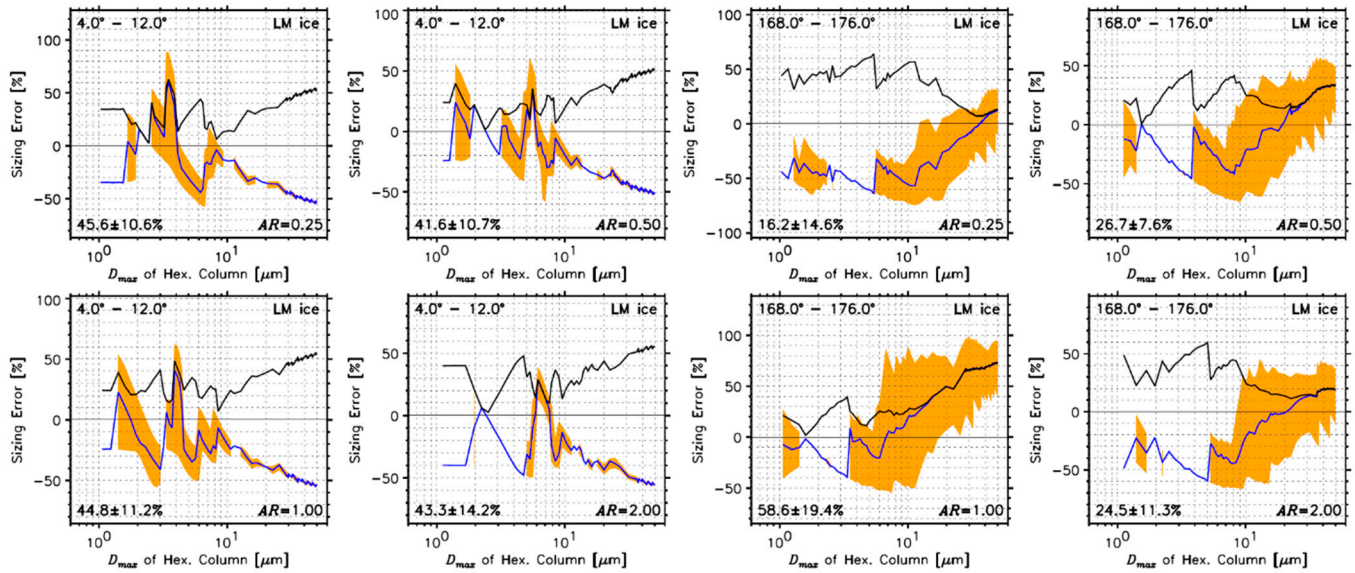

Figure 9. The same as Figure 8, but spherical ice cloud droplets were assumed for the Lorenz–Mie calculations (LM ice).

4.2.3. Determined Sizing Errors Using Hexagonal Ice Crystals

The fourth case considered is that the current forward scattering probe (i.e., CAS) measures hexagonal ice crystals whose sizes are determined using the exact calculations of forward and backward scattering cross-sections of hexagonal ice crystals with AR = 0.25, 0.50, 1.00, and 2.00 (denoted as "All ARs" in Table 3) using the ADDA (i.e., red lines in Figures 4 and 5). Thus, this is a new size conversion table of ice crystals for forward scattering probes.

The determined average ± standard deviation (maximum) of sizing errors of hexagonal ice crystals shown in Figure 10 and Table 3 are 15.7 ± 14.4% (106.7%), 14.3 ± 10.1% (103.3%), 12.0 ± 8.5% (69.1%), and 14.7 ± 10.2% (82.5%) for AR = 0.25, 0.50, 1.00, and 2.00, respectively, in the forward direction. The sizing errors in the backward direction are larger than those in the forward direction, and are 18.7 ± 3.9% (46.6%), 19.3 ± 7.4% (74.3%), 33.5 ± 8.6% (86.7%), and 15.9 ± 3.4% (37.5%). The determined sizing errors using a newly developed size conversion table are reduced significantly compared to those determined using spherical liquid water droplets shown in Section 4.2.1. Table 3 shows that computations using the best-fit calculation, in general, improve the average of sizing errors (figures are not shown).

Figure 11 and the bottom row of Table 3 shows the determined average ± standard deviation (maximum) of sizing errors of hexagonal ice crystals with AR = 1.0 only, which differs from Figure 10. This is a more conservative test since small ice crystals may have compact shapes whose ARs are close to unity. In this case, the determined average ± standard deviations (maximum) of the sizing errors are 5.6 ± 8.8% (64.9%) in the forward direction and there are no errors in the backward direction. Since the backward scattering cross-sections of AR = 1.0 (see Figure 5) has a linear increment, multiple particle sizes are not determined and hence, there were no errors. This result implies that sizing errors caused by possible multiple particle sizes can be reduced by selecting optimal scattering angles where the differential scattering cross-sections of cloud particles increase monotonically with size, as shown in Section 5.

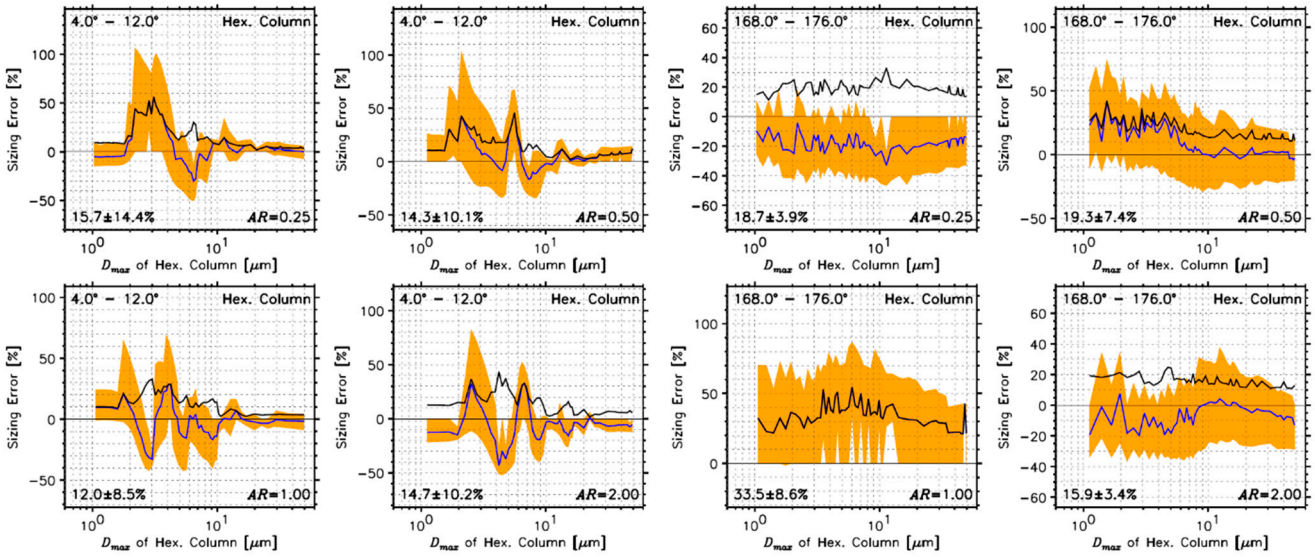

Figure 10. Determined sizing errors of hexagonal ice crystals in forward (4–12°, **left two columns**) and backward (168–176°, **right two columns**) directions. The sizing errors are calculated using an exact comparison between the measured D_{max} of hexagonal ice crystals and those calculated by the ADDA assuming hexagonal ice crystals. Each panel represents a different aspect ratio of a hexagonal ice crystal. The color scheme is the same as Figure 6.

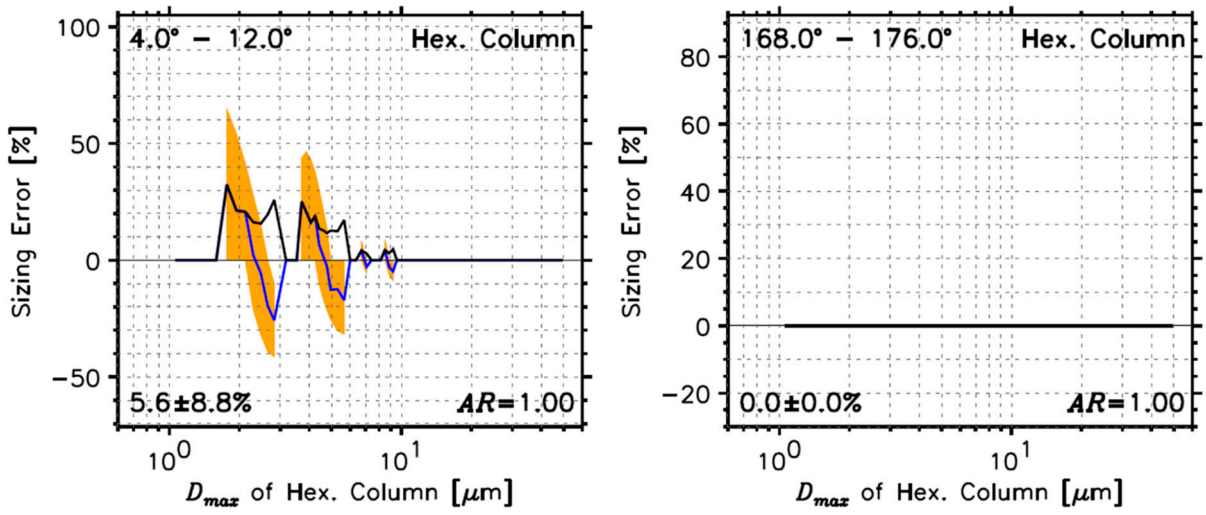

Figure 11. Determined sizing errors of hexagonal ice crystals in forward (4–12°, **left**) and backward (168–176°, **right**) directions. The sizing errors are calculated using an exact comparison between the measured D_{max} of hexagonal ice crystals and those calculated by the ADDA assuming hexagonal ice crystals with aspect ratio of 1.0. The color scheme is the same as Figure 6.

5. Determined Optimal Scattering Angles for Forward Scattering Probes

To find the optimal scattering angles, a pair of scattering angles (θ_1 and θ_2) was varied with a resolution of 1°, 2°, 4°, 6°, or 8° between 0° and 180° with a 1° increment. For each pair of scattering angles with a given resolution, sizing errors were calculated, and optimal scattering angles were determined in terms of an average and maximum of sizing errors.

5.1. Optimal Scattering Angles for Spherical Liquid Cloud Droplets

Figure 12 shows the calculated sizing errors as functions of scattering angles and size of spherical liquid cloud droplets. Different panels indicate different resolutions (i.e., 2°, 4°, 6°, and 8°) of scattering angles. It should be noted that the calculated sizing error is plotted at θ_1. For example, the determined sizing error between θ_1 = 4° and θ_2 = 12° for the 8° resolution is plotted at θ_1 = 4°. Thus, sizing errors were not available to calculate for some scattering angles and, for example, the last pair of scattering angles that was calculated is θ_1 = 172° and θ_2 = 180° for the 8° resolution, which is plotted at θ_1 = 172°. The same calculations were applied to Figures 12–18.

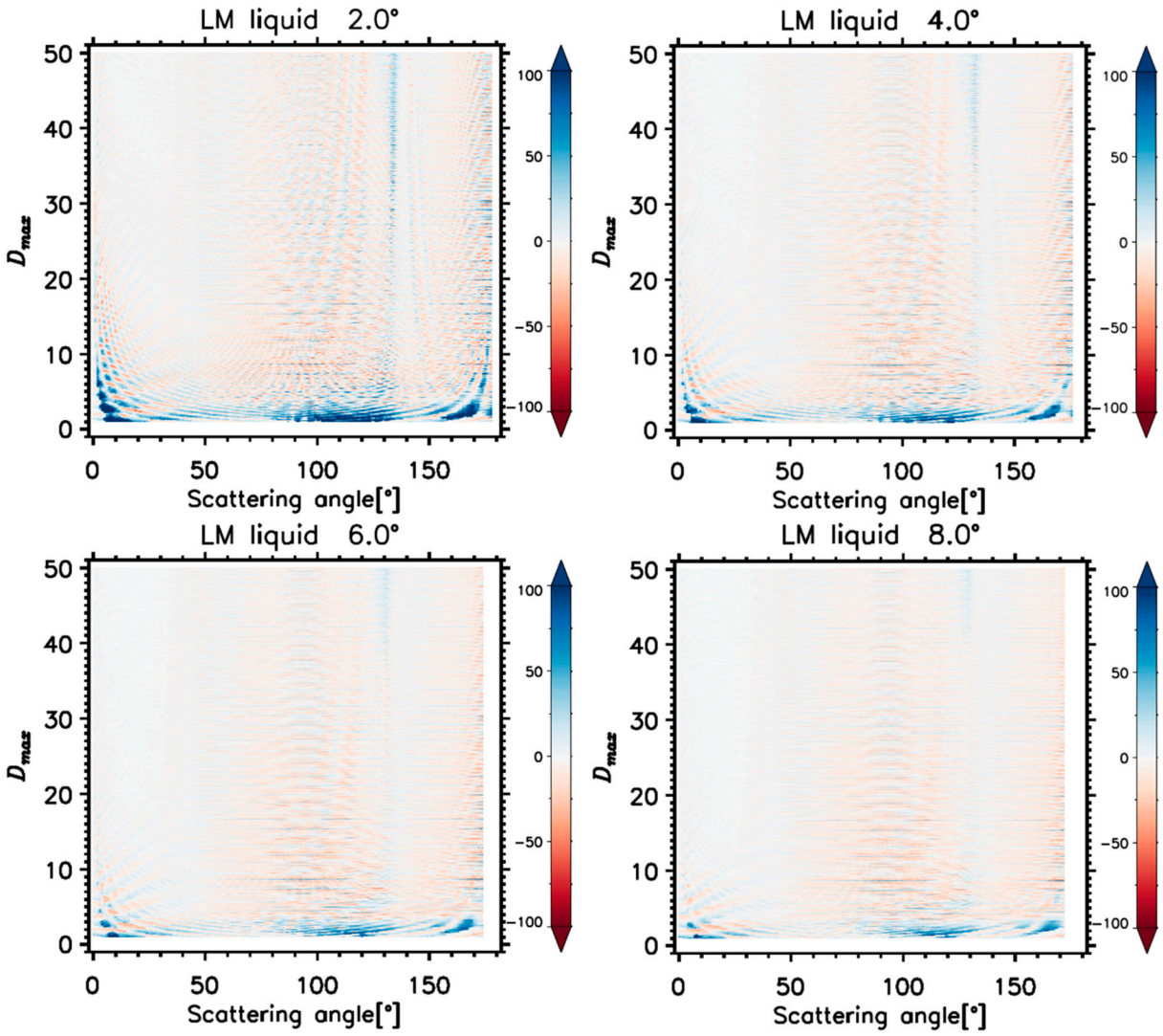

Figure 12. Determined sizing errors (%) of spherical liquid cloud droplets using a Lorenz–Mie code (LM liquid) as functions of scattering angles and the size (D_{max}). Different panels indicate different resolutions (i.e., 2°, 4°, 6°, and 8°) of scattering angles.

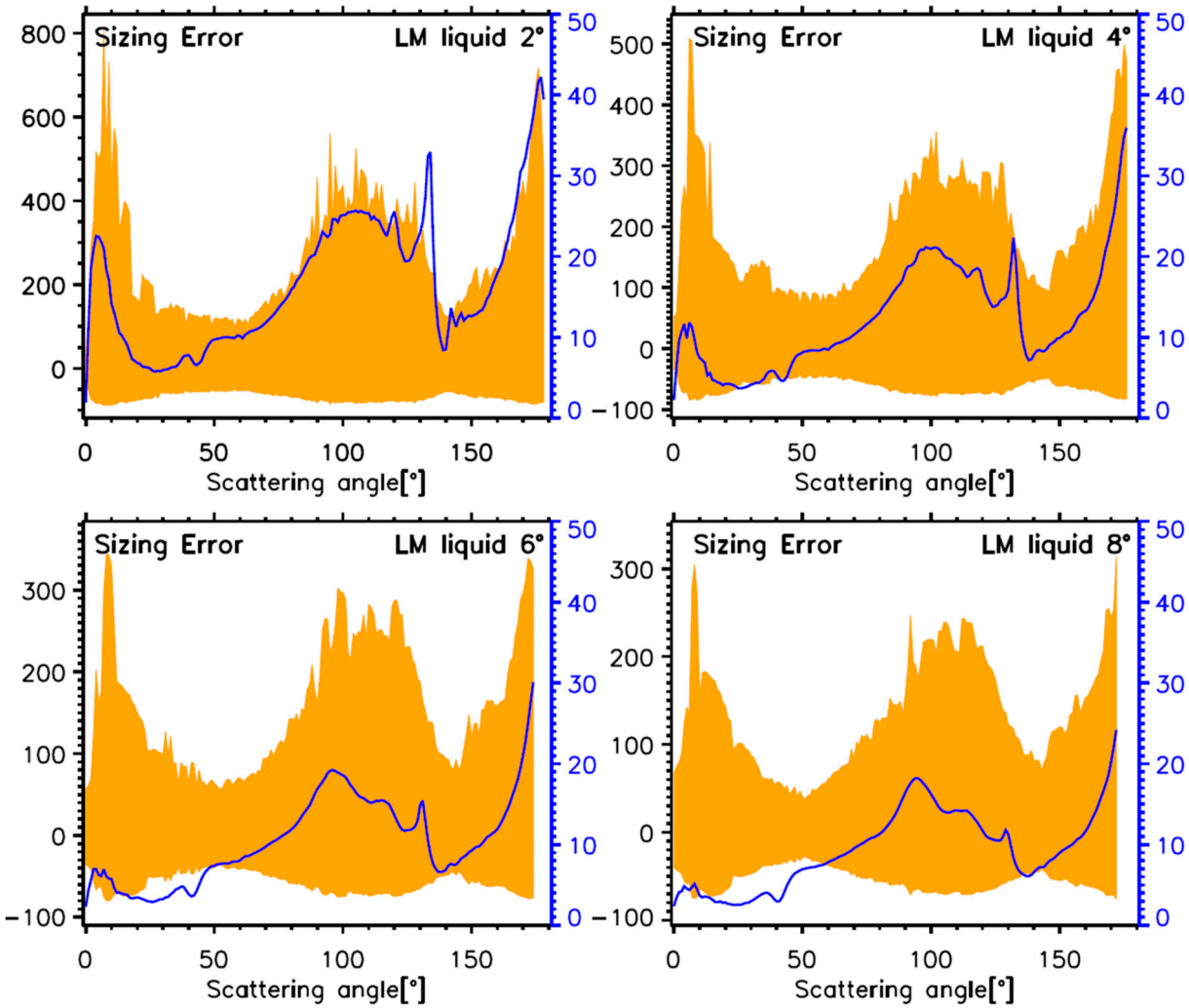

Figure 13. Determined ranges (orange shaded areas, left vertical axis) of minima and maxima and average (blue lines, right vertical axis) of sizing errors (%) for measured spherical liquid cloud droplets using a Lorenz–Mie code (LM liquid) as a function of scattering angle. Different panels indicate different resolutions (i.e., 2°, 4°, 6°, and 8°) of scattering angles.

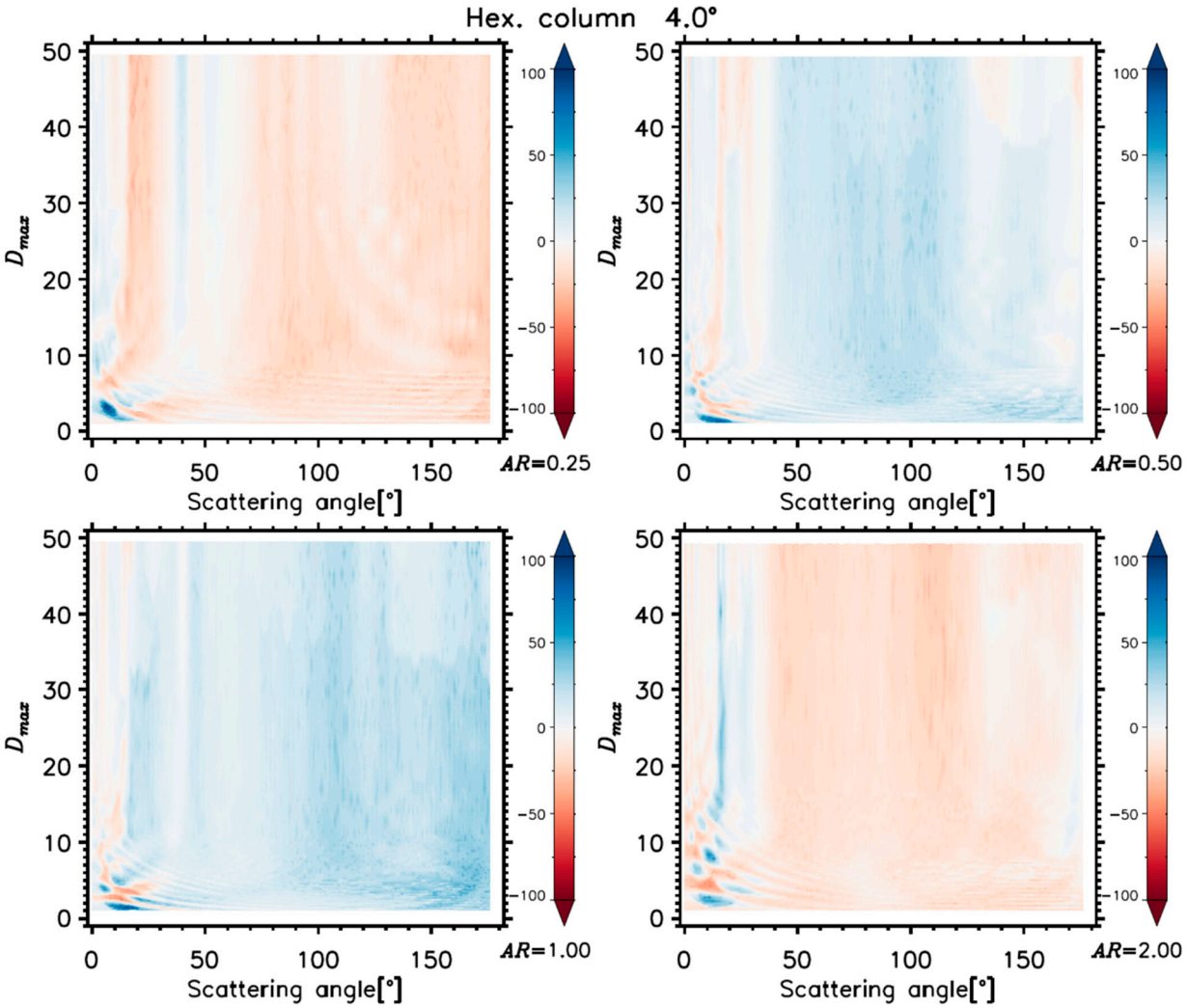

Figure 14. Determined sizing errors (%) as functions of scattering angles and the size (D_{max}) of hexagonal ice crystals with AR = 0.25, 0.50, 1.00, and 2.00 using the ADDA for 4° resolution of scattering angles.

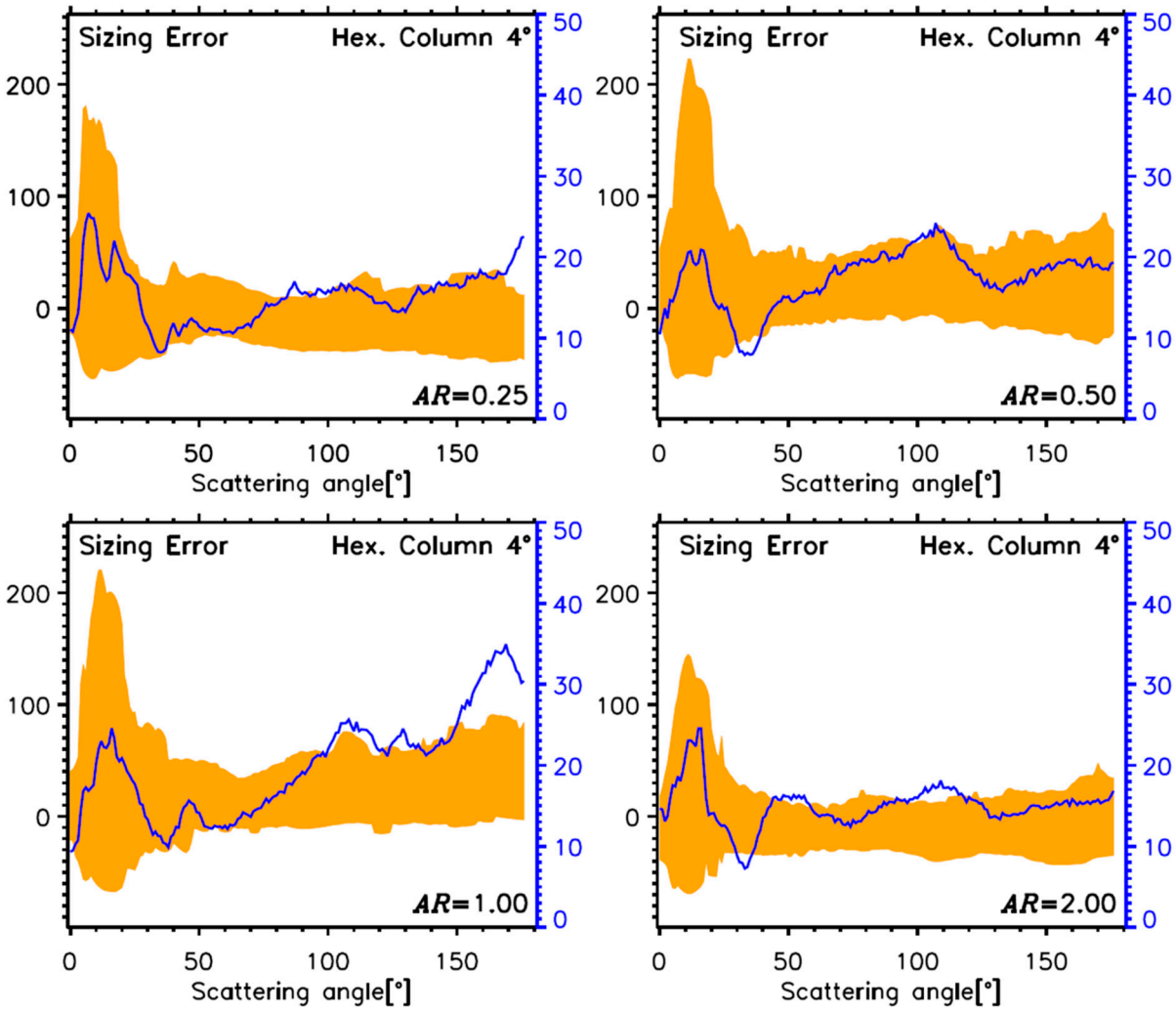

Figure 15. Determined ranges (orange shaded areas, left vertical axis) of minima and maxima and average (blue lines, right vertical axis) of sizing errors (%) for measured hexagonal ice crystals with *AR* = 0.25, 0.50, 1.00, and 2.00 using the ADDA as a function of scattering angle. The 4° resolution of scattering angles are shown.

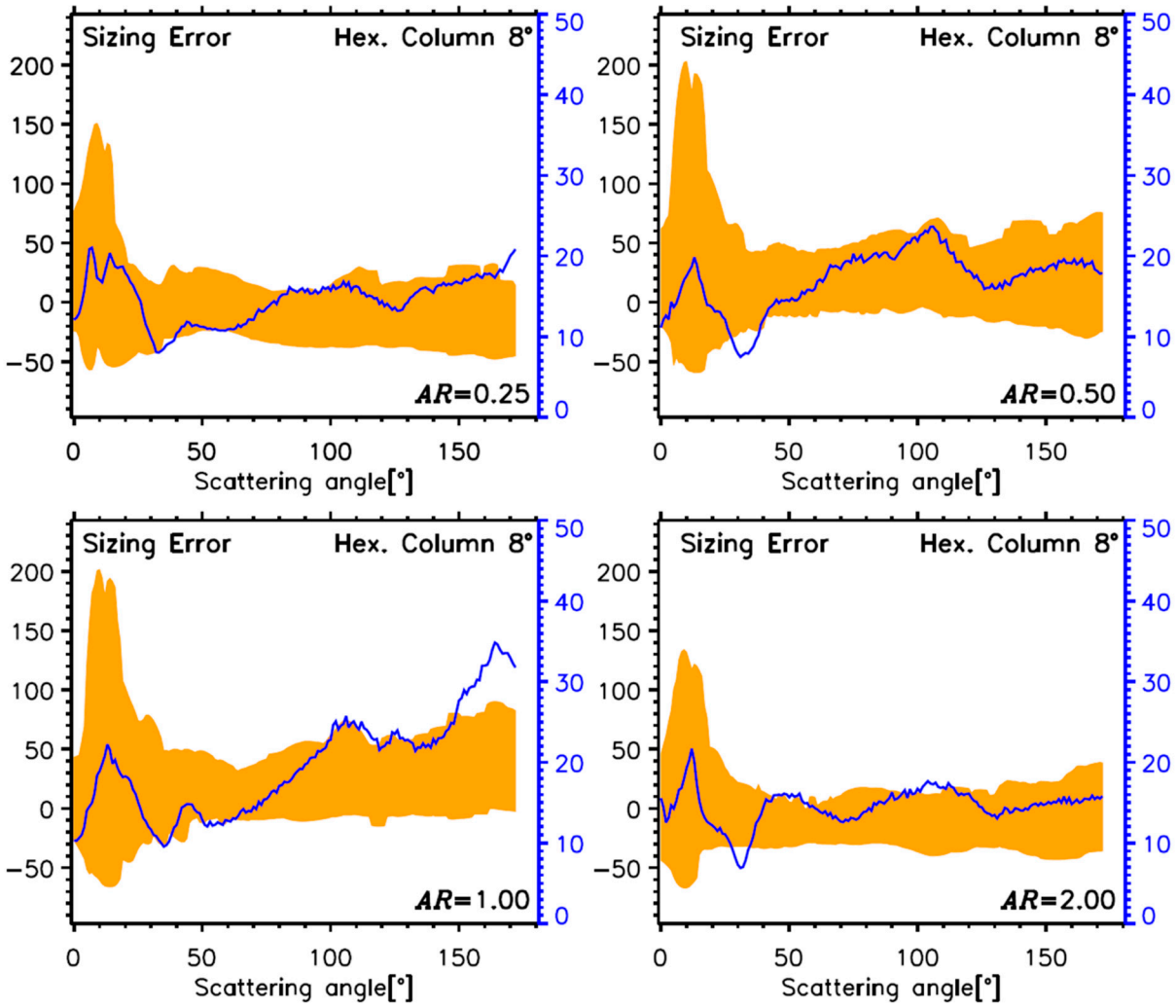

Figure 16. The same as Figure 15, but for 8° resolution of scattering angles.

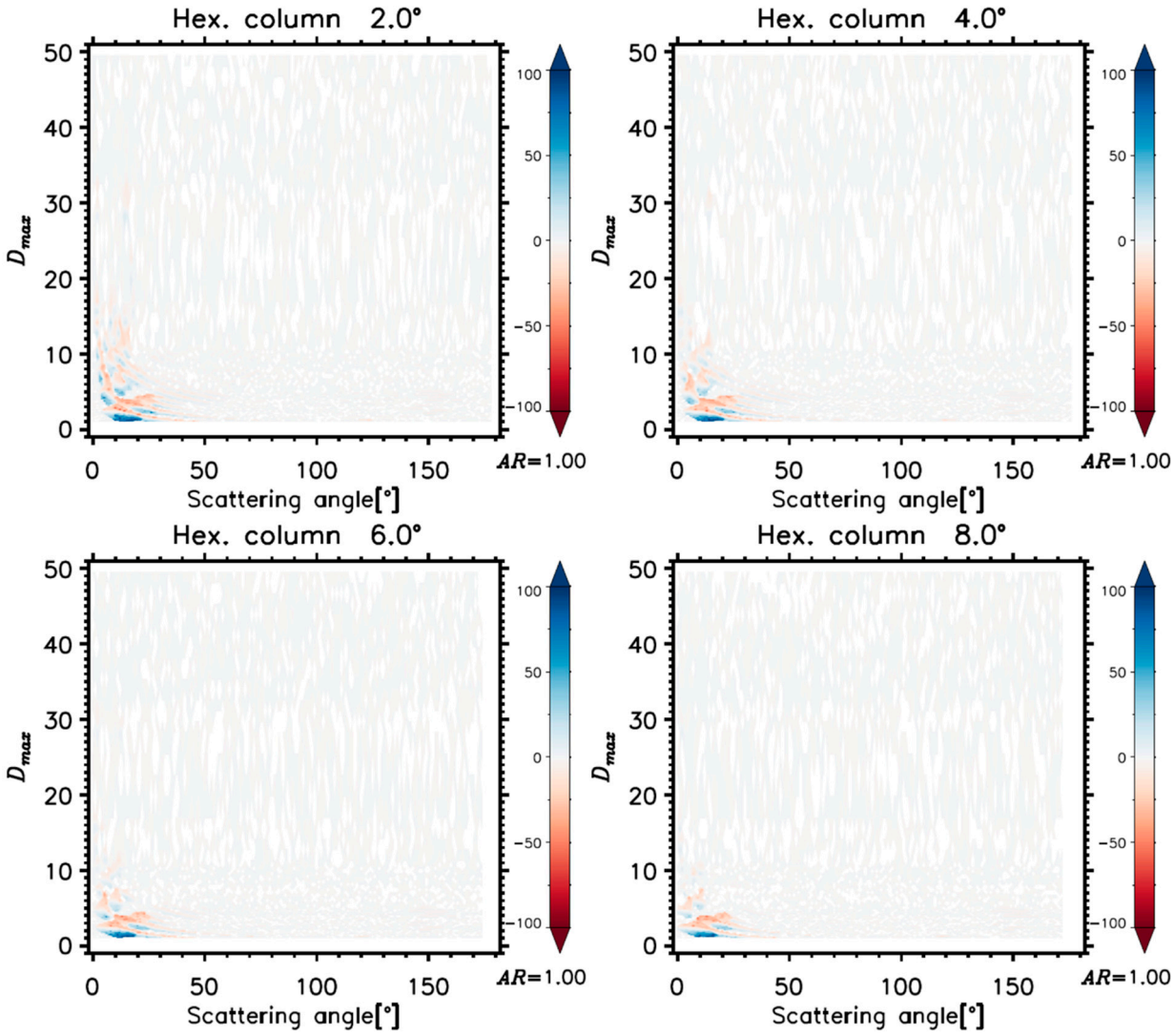

Figure 17. Determined sizing errors (%) as functions of scattering angles and the size (D_{max}) of hexagonal ice crystals with AR = 1.00 only using the ADDA. Different panels indicate different resolutions (i.e., 2°, 4°, 6°, and 8°) of scattering angles.

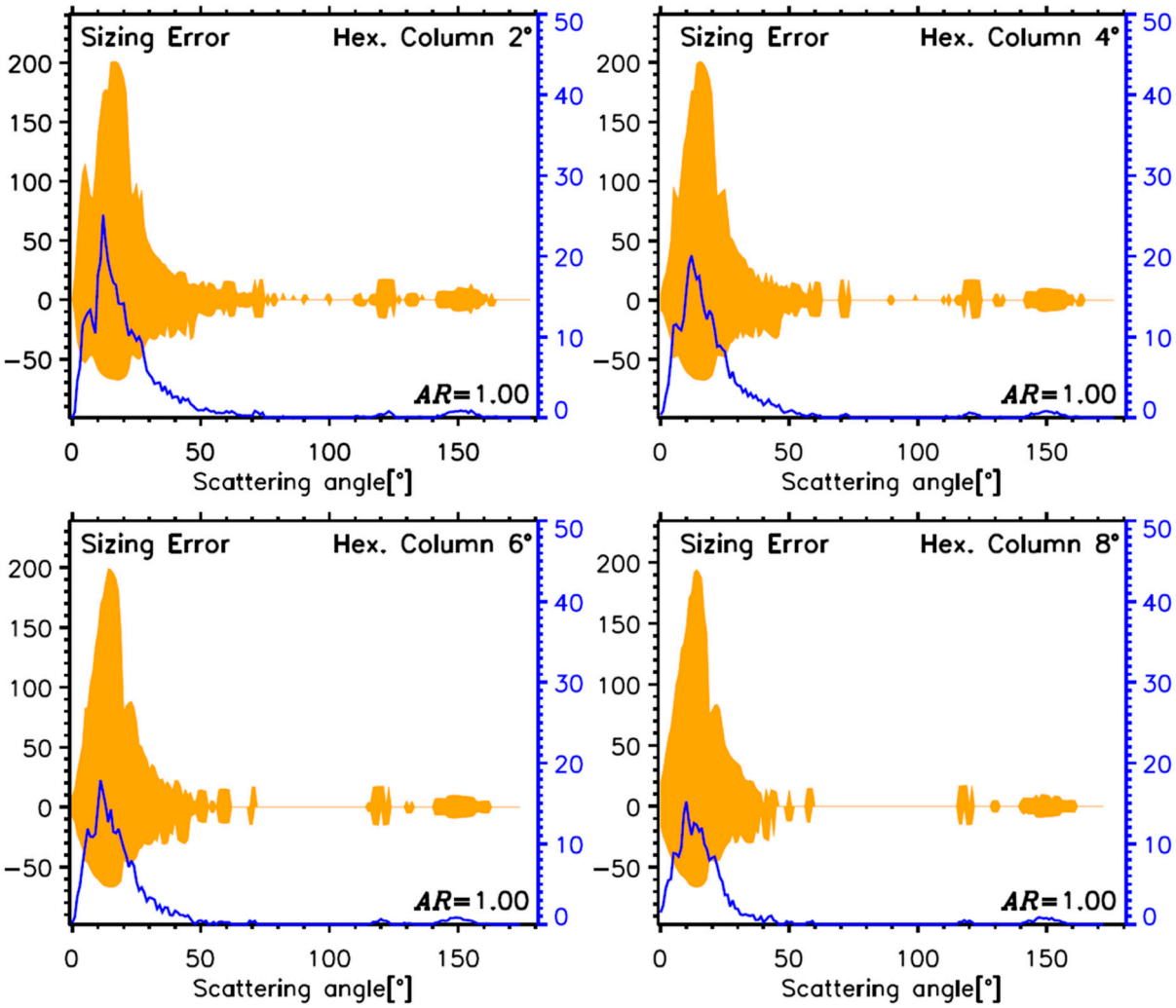

Figure 18. Determined ranges (orange shaded areas, left vertical axis) of minima and maxima and average (blue lines, right vertical axis) of sizing errors (%) for measured hexagonal ice crystals with *AR* = 1.00 only using the ADDA as a function of scattering angle. Different panels indicate different resolutions (i.e., 2°, 4°, 6°, and 8°) of scattering angles.

Overestimations (i.e., blue color) of the determined sizes for smaller particles (D_{max} < ~10 μm) are distinct due to the Mie ambiguity. Complex mixtures of overestimation and underestimation patterns elsewhere are shown in Figure 12. Overestimations due to the primary and secondary rainbow peaks in P_{11} are shown at scattering angles between 130° and 140°, which are more distinct for larger particles. At λ = 0.55 μm, the primary and secondary rainbow peak is ~137.9° and ~129.1°, respectively. The overestimations due to the primary and secondary rainbow peaks are reduced and some of other sizing errors are smoothed out as the resolution of scattering angles increases. The determined sizing errors using a finer resolution (i.e., 1°) show more complex mixtures of overestimation and underestimation patterns (figure not shown), which does not improve the sizing error.

Figure 13 shows the ranges of the minima and maxima (enclosed by orange areas) of sizing errors of the measured spherical liquid cloud droplets, while the blue lines indicate an average of the absolute values of all sizing errors for a given size of a particle. The sizing errors associated with the primary and secondary rainbow peaks are distinct at scattering angles between 130° and 140°, especially for the 2° resolution, which is reduced for the coarser resolutions. Four different resolutions (i.e., 2°, 4°, 6°, and 8°) of scattering angles show that sideward (~70–~140°) and backward (~170–~180°) directions are not suitable for use as scattering angles of forward scattering probes.

In Section 4.1, it was shown that current forward scattering probe (i.e., CAS) has 5.0 ± 9.7% (121.9%) of average ± standard deviation (maximum) errors in sizing spherical liquid cloud droplets at forward scattering angles (4–12°). To reduce the difference between maximum and minimum errors (i.e., standard deviation), a selection of scattering angles between 51° and 59° is the best selection, which provides the average ± standard deviation (maximum) of sizing errors of 7.0 ± 2.6% (37.4%). Alternatively, to improve the average sizing errors, a selection of scattering angles between 23° and 31° provides sizing errors of 2.5 ± 5.2% (95.2%), which is half of the average sizing errors (i.e., 5.0%) of current forward scattering probes.

5.2. Optimal Scattering Angles for Hexagonal Ice Crystals

Figure 14 shows the calculated sizing errors as functions of scattering angles and size (i.e., D_{max}) of hexagonal ice crystals with AR = 0.25, 0.50, 1.00, and 2.00 using the ADDA. Different panels indicate different ARs of hexagonal ice crystals. Compact shapes (i.e., AR = 0.50 and 1.00) of hexagonal ice crystals show greater overestimation of size, while greater underestimations are revealed for oblate (AR = 0.50) and prolate (AR = 2.00) shapes. Complex mixtures of overestimation and underestimation are found for smaller crystals (D_{max} < ~15 μm) and for scattering angles less than ~30°. Sizing errors associated with 22° and 46° halo peaks are also shown.

Figures 15 and 16 show the ranges of minima and maxima (enclosed by orange areas) and the average of the absolute values of all sizing errors for a given size of a particle with different resolutions of scattering angles. For all four ARs, scattering angles smaller than 20° are not suitable selections. For AR = 1.00 the sizing errors increase with scattering angles >~50°.

In Section 4.2.3, it was shown that the determined average ± standard deviation (maximum) of sizing errors of hexagonal ice crystals were 15.7 ± 14.4% (106.7%), 14.3 ± 10.1% (103.3%), 12.0 ± 8.5% (69.1%), and 14.7 ± 10.2% (82.5%) for AR = 0.25, 0.50, 1.00, and 2.00, respectively, in the forward direction. To reduce the difference between maximum and minimum errors (i.e., standard deviation), scattering angles of 79–83° (60–64°; 64–72°; 64–68°) provide sizing errors of 14.1 ± 4.0% (34.3%), 15.6 ± 3.0% (40.8%), 13.3 ± 2.2% (31.9%), and 13.8 ± 2.8% (28.9%) for AR = 0.25 (0.50; 1.00; 2.00), respectively. Alternatively, to improve the average sizing errors, selections of scattering angles with 33–41° (31–39°; 35–43°; 32–40°) provide sizing errors of 8.0 ± 5.6% (41.4%), 7.5 ± 5.6% (62.3%), 9.5 ± 5.5% (48.8%), and 7.0 ± 4.6% (31.9%) for AR = 0.25 (0.50; 1.00; 2.00), respectively.

The calculations using hexagonal ice crystals with AR = 1.00 only are shown in Figures 17 and 18. Most sizing errors are concentrated at smaller scattering angles and for smaller sizes (see Figure 17). It is shown that any selection of scattering angles >~50° would reduce sizing errors.

To summarize, scattering angles between approximately 30–40° (60–70°) are suitable selections to reduce the averages (standard deviations) of sizing errors of hexagonal ice crystals with AR = 0.25, 0.50, 1.00, and 2.00 using the ADDA. For compact shapes (i.e., AR = 1.00) of hexagonal ice crystals, any selection of scattering angles larger than >~50° would effectively reduce the sizing errors.

6. Conclusions

In this study, the directional scattering intensities of cloud droplets (i.e., liquid cloud droplets and hexagonal ice crystals) with D_{max} < 50 μm were calculated using a Lorenz–Mie code and ADDA to quantify the impact of nonsphericity on the measurement accuracy of forward scattering probes to examine whether the ranges of forward and backward scattering angles that are currently used in forward scattering probes are suitable to measure sizes of small ice crystals and liquid cloud droplets. In addition, these calculations helped to determine the optimal scattering angles in the forward and backward directions that minimize the sizing errors for future versions of forward scattering probes. This study is a purely theoretical examination of the operating principle of forward scattering probes

excluding any calibration technique method and processing technique developed to reduce sizing errors. The most important findings of this study are summarized below:

1. The current forward scattering probes (i.e., CAS) have 5.0 ± 9.7% (121.9%) of average ± standard deviation (maximum) errors in sizing liquid cloud droplets in the forward direction (4–12°), with errors of 17.4 ± 12.8% (229.2%) in the backward direction (168–176°).
2. For measurements of hexagonal ice crystals, sizing errors were 44.2 ± 10.1% (91.3%), 40.2 ± 10.1% (58.8%), 43.0 ± 11.7% (59.3%), and 41.1 ± 15.3 (55.4%) for AR = 0.25, 0.50, 1.00, and 2.00, respectively, in the forward direction, and 20.6±16.1% (74.8%), 15.5 ± 9.0% (66.5%), 39.7 ± 10.1% (70.8%), and 19.6 ± 18.2% (67.9%) in the backward direction based on the calculations using a Lorenz–Mie code with assumptions of liquid spherical cloud droplets.
3. It was shown that the errors in sizing ice crystals using current forward scattering probes increased almost linearly for D_{max} > ~8 μm in the forward direction (4–12°), which implies larger sizing errors for larger ice crystals.
4. Replacing spherical liquid cloud droplets with spherical ice cloud droplets did not improve the sizing errors. Thus, the impact of the shape of an ice crystal is larger than that of the thermodynamic phase for measurements of forward scattering probes.
5. A newly developed size conversion table based on the ADDA calculations reduced the sizing errors of hexagonal ice crystals to 15.7 ± 14.4% (106.7%), 14.3 ± 10.1% (103.3%), 12.0 ± 8.5% (69.1%), and 14.7 ± 10.2% (82.5%) for AR = 0.25, 0.50, 1.00, and 2.00, respectively, in the forward direction, while those were 18.7 ± 3.9% (46.6%), 19.3 ± 7.4% (74.3%), 33.5 ± 8.6% (86.7%), and 15.9 ± 3.4% (37.5%) in backward direction.
6. It was shown that the determined optimal scattering angles were 23–31° (51–59°) to minimize the average (standard deviation) of sizing errors, which provided 2.5 ± 5.2% (7.0 ± 2.6%) of average ± standard deviation errors in sizing liquid cloud droplets.
7. Approximately, the 30–40° (60–70°) were suitable selections to reduce the averages (standard deviations) of sizing errors of hexagonal ice crystals with AR = 0.25, 0.50, 1.00, and 2.00 using the ADDA.
8. For compact shapes (i.e., AR = 1.00) of hexagonal ice crystals, any selection of scattering angles larger than >~50° would effectively reduce the sizing errors based on the ADDA calculations.

This study quantified the errors in sizing small ice crystals and cloud droplets using current forward scattering probes and determined the ranges of optimal scattering angles that would be used in future forward scattering probes. It was shown that a newly developed size conversion table using hexagonal ice crystals reduced the sizing errors significantly compared to those determined using spherical liquid water droplets. Since several high temporal or particle-by-particle phase discrimination techniques are available [75,76], it is worth attempting to determine the sizes of spherical liquid cloud droplets and nonspherical ice crystals using different size conversion tables for forward scattering probes. The suggested optimal scattering angles for spherical liquid cloud droplets and ice crystals can be the theoretical basis for developing the next generation of forward scattering probes. There would be many difficulties, of course, to realize the suggested scattering angles due to the limitations, such as probe design (e.g., avoiding shattering), optical mounting, and sensitivity of the laser beam and optical sensors (e.g., low signal-to-noise ratios in larger scattering angles). However, more than half of a century has passed since the development of the original version of forward scattering probes, it seems that most of these limitations have been overcome.

It should be emphasized that this study is a purely theoretical examination of the operating principle of forward-scattering probes. It should also be emphasized that numerous efforts have been made to develop calibration methods and processing techniques to reduce the measurement uncertainties of forward scattering probes, which were not considered in this study. A limitation of this study might be the assumption of simple

shapes of hexagonal ice crystals with smooth surfaces. Although the hexagonal lattice structure is the basic structure of small ice crystals, at least for diffusionally growing crystals, there is considerable variability in the shapes of large ice crystals with many other crystal shapes also present. For dissipating (i.e., sublimation) small ice crystals the surface roughness of small ice crystals is highly uncertain. The impacts of surface roughness might be weak in forward directions, but they can be large in backward directions [77,78]. Thus, there are still large uncertainties to characterize the shapes and surface roughness of dissipating small ice crystals. Further, the assumption of hexagonal ice crystals with random orientations to calculate the single-scattering properties of small ice crystals might be not adequate for the measurements of forward-scattering probes. Nonsphericity of ice crystal causes the dependence of single-scattering properties on particle orientation, which was not covered in this study and will be the research subject of a subsequent study. The development of a new cloud probe that can distinguish the three-dimensional shapes of small ice crystals to be used in lab studies and in situ observations is necessary to advance our knowledge of the cloud physics, which is demanded by the cloud and precipitation modelling community [79].

Author Contributions: Conceptualization, J.U. and G.M.M.; methodology, J.U.; formal analysis, S.J., S.S.L., C.H.J., S.S.P. and J.U.; data curation, S.J., J.K., S.P., S.S.L., C.H.J., S.S.P., J.W.C. and K.L.; writing-original draft preparation, S.J., J.K., G.M.M., S.P., S.S.L., C.H.J., S.S.P., J.W.C., K.L. and J.U.; writing—review and editing, S.J., J.K., G.M.M., S.P. and J.U.; visualization, S.J., J.K., S.P. and S.S.P. All authors have read and agreed to the published version of the manuscript.

Funding: This research was supported by the National Research Foundation of Korea (NRF) grant funded by the Korean government (MSIT) (No. 2020R1A2C1013278 and No. 2020R1A2C1003215) and by Basic Science Research Program through the NRF funded by the Ministry of Education (No. 2020R1A6A1A03044834). This work was funded by the Korea Meteorological Administration Research and Development Program "Research on Weather Modification and Cloud Physics" under Grant (KMA2018-00224).

Acknowledgments: This study was conducted employing the system of Korea Meteorological Institute, communally used by weather and climate industry. We thank M. Yurkin for the ADDA code and C.F. Bohen and D.R. Huffman for the Lorenz-Mie code.

Conflicts of Interest: The authors declare no conflict of interest.

References

1. Bailey, M.; Hallett, J. Growth rates and habits of ice crystals between −20 °C and −70 °C. *J. Atmos. Sci.* **2004**, *61*, 514–544. [CrossRef]
2. Um, J.; McFarquhar, G.M. Dependence of the single-scattering properties of small ice crystals on idealized shape models. *Atmos. Chem. Phys.* **2011**, *11*, 3159–3171. [CrossRef]
3. Um, J.; McFarquhar, G.M. Formation of atmospheric halos and applicability of geometric optics for calculating single-scattering properties of hexagonal ice crystals: Impacts of aspect ratio and ice crystal size. *J. Quant. Spectrosc. Radiat. Transf.* **2015**, *165*, 134–152. [CrossRef]
4. Knollenberg, R.G. The optical array: An alternative to scattering or extinction for airborne particle size determination. *J. Appl. Meteor.* **1970**, *9*, 86–103. [CrossRef]
5. Baumgardner, D.; Jonsson, H.; Dawson, W.; O'Connor, D.; Newton, R. The cloud, aerosol and precipitation spectrometer: A new instrument for cloud investigations. *Atmos. Res.* **2001**, *59–60*, 251–264. [CrossRef]
6. Lawson, R.P.; Stewart, R.E.; Angus, L.J. Observations and numerical simulations of the origin and development of very large snowflakes. *J. Atmos. Sci.* **1998**, *55*, 3209–3229. [CrossRef]
7. Lawson, R.P.; O'Connor, D.; Zmarzly, P.; Weaver, K.; Baker, B.; Mo, Q.; Jonsson, H. The 2DS (stereo) probe: Design and preliminary tests of a new airborne, high speed, high-resolution particle imaging probe. *J. Atmos. Ocean. Tech.* **2006**, *23*, 1462–1471. [CrossRef]
8. Baumgardner, D.; Abel, S.J.; Axisa, D.; Cotton, R.; Crosier, J.; Field, P.; Gurganus, C.; Heymsfield, A.; Korolev, A.; Krämer, M.; et al. Cloud ice properties: In situ measurement challenges. *Meteor. Monogr.* **2017**, *58*, 9.1–9.23. [CrossRef]
9. Gurganus, C.; Lawson, P. Laboratory and Flight Tests of 2D Imaging Probes: Toward a Better Understanding of Instrument Performance and the Impact on Archived Data. *J. Atmos. Ocean. Tech.* **2018**, *35*, 1533–1553. [CrossRef]
10. Wendisch, M.; Brenguier, J.-L. *Airborne Measurements for Environmental Research: Methods and Instruments*; John Wiley & Sons: New York, NY, USA, 2013.

11. McFarquhar, G.M.; Baumgardner, D.; Bansemer, A.; Abel, S.J.; Crosier, J.; French, J.; Rosenberg, P.; Korolev, A.; Schwarzoenboeck, A.; Leroy, D.; et al. Processing of Ice Cloud In Situ Data Collected by Bulk Water, Scattering, and Imaging Probes: Fundamentals, Uncertainties, and Efforts toward Consistency. *Meteor. Monogr.* **2017**, *58*, 11.1–11.33. [CrossRef]
12. Faber, S.; French, J.R.; Jackson, R. Laboratory and in-flight evaluation of measurement uncertainties from a commercial Cloud Droplet Probe (CDP). *Atmos. Meas. Tech.* **2018**, *11*, 3645–3659. [CrossRef]
13. Pinnick, R.G.; Garvey, D.M.; Duncan, L.D. Calibration of Knollenberg FSSP Light-Scattering Counters for Measurement of Cloud Droplets. *J. Appl. Meteor. Climatol.* **1981**, *20*, 1049–1057. [CrossRef]
14. Dye, J.E.; Baumgardner, D. Evaluation of the forward scattering spectrometer probe. Part I: Electronic and optical studies. *J. Atmos. Ocean. Tech.* **1984**, *1*, 329–344. [CrossRef]
15. Spiegel, J.K.; Zieger, P.; Bukowiecki, N.; Hammer, E.; Weingartner, E.; Eugster, W. Evaluating the capabilities and uncertainties of droplet measurements for the fog droplet spectrometer (FM-100). *Atmos. Meas. Tech.* **2012**, *5*, 2237–2260. [CrossRef]
16. Cox, C.J.; Noone, D.C.; Berkelhammer, M.; Shupe, M.D.; Neff, W.D.; Miller, N.B.; Walden, V.P.; Steffen, K. Supercooled liquid fogs over the central Greenland Ice Sheet. *Atmos. Chem. Phys.* **2019**, *19*, 7467–7485. [CrossRef]
17. Um, J. Calculations of Optical Properties of Cloud Particles to Improve the Accuracy of Forward Scattering Probes for In-Situ Aircraft Cloud Measurements. *Atmosphere* **2020**, *30*, 75–89.
18. Lance, S.; Brock, C.A.; Rogers, D.; Gordon, J.A. Water droplet calibration of the cloud droplet probe (CDP) and in-flight performance in liquid, ice and mixed-phase clouds during ARCPAC. *Atmos. Meas. Tech.* **2010**, *3*, 1683–1706. [CrossRef]
19. Hovenac, E.A.; Hirleman, E.D. Use of Rotating Pinholes and Reticles for Calibration of Cloud Droplet Instrumentation. *J. Atmos. Ocean. Tech.* **1991**, *8*, 166–171. [CrossRef]
20. Rosenberg, P.D.; Dean, A.R.; Williams, P.I.; Dorsey, J.R.; Minikin, A.; Pickering, M.A.; Petzold, A. Particle sizing calibration with refractive index correction for light scattering optical particle counters and impacts upon PCASP and CDP data collected during the Fennec campaign. *Atmos. Meas. Tech.* **2012**, *5*, 1147–1163. [CrossRef]
21. Mishchenko, M.I.; Travis, L.D.; Lacis, A.A. *Scattering, Absorption, and Emission of Light by Small Particles*; Cambridge University Press: Campridge, UK, 2002.
22. Baumgardner, D.; Strapp, W.; Dye, J.E. Evaluation of the Forward Scattering Spectrometer Probe. Part II: Corrections for Coincidence and Dead-Time Losses. *J. Atmos. Ocean. Tech.* **1985**, *2*, 626–632. [CrossRef]
23. Cooper, W.A. Effects of Coincidence on Measurements with a Forward Scattering Spectrometer Probe. *J. Atmos. Ocean. Tech.* **1988**, *5*, 823–832. [CrossRef]
24. Burnet, F.; Brenguier, J. Comparison between Standard and Modified Forward Scattering Spectrometer Probes during the Small Cumulus Microphysics Study. *J. Atmos. Ocean. Tech.* **2002**, *19*, 1516–1531. [CrossRef]
25. Cotton, R.; Osborne, S.; Ulanowski, Z.; Hirst, E.; Kaye, P.H.; Greenaway, R.S. The Ability of the Small Ice Detector (SID-2) to Characterize Cloud Particle and Aerosol Morphologies Obtained during Flights of the FAAM BAe-146 Research Aircraft. *J. Atmos. Ocean. Tech.* **2010**, *27*, 290–303. [CrossRef]
26. Lance, S. Coincidence Errors in a Cloud Droplet Probe (CDP) and a Cloud and Aerosol Spectrometer (CAS), and the Improved Performance of a Modified CDP. *J. Atmos. Ocean. Tech.* **2012**, *29*, 1532–1541. [CrossRef]
27. Johnson, A.; Lasher-Trapp, S.; Bansemer, A.; Ulanowski, Z.; Heymsfield, A.J. Difficulties in Early Ice Detection with the Small Ice Detector-2 HIAPER (SID-2H) in Maritime Cumuli. *J. Atmos. Ocean. Tech.* **2014**, *31*, 1263–1275. [CrossRef]
28. Gardiner, B.A.; Hallett, J. Degradation of In-Cloud Forward Scattering Spectrometer Probe Measurements in the Presence of Ice Particles. *J. Atmos. Ocean. Tech.* **1985**, *2*, 171–180. [CrossRef]
29. Field, P.R.; Wood, R.; Brown, P.R.A.; Kaye, P.H.; Hirst, E.; Greenaway, R.; Smith, J.A. Ice Particle Interarrival Times Measured with a Fast FSSP. *J. Atmos. Ocean. Tech.* **2003**, *20*, 249–261. [CrossRef]
30. Heymsfield, A.J. On measurements of small ice particles in clouds. *Geophys. Res. Lett.* **2007**, *34*, L23812. [CrossRef]
31. McFarquhar, G.M.; Um, J.; Freer, M.; Baumgardner, D.; Kok, G.L.; Mace, G. Importance of small ice crystals to cirrus properties: Observations from the Tropical Warm Pool International Cloud Experiment (TWP-ICE). *Geophys. Res. Lett.* **2007**, *34*, L13803. [CrossRef]
32. Baker, B.; Mo, Q.; Lawson, R.P.; O'Connor, D.; Korolev, A. The Effects of Precipitation on Cloud Droplet Measurement Devices. *J. Atmos. Ocean. Tech.* **2009**, *26*, 1404–1409. [CrossRef]
33. Korolev, A.V.; Emery, E.F.; Strapp, J.W.; Cober, S.G.; Isaac, G.A.; Wasey, M.; Marcotte, D. Small Ice Particles in Tropospheric Clouds: Fact or Artifact? Airborne Icing Instrumentation Evaluation Experiment. *Bull. Amer. Meteor. Soc.* **2011**, *92*, 967–973. [CrossRef]
34. Korolev, A.V.; Emery, E.F.; Strapp, J.W.; Cober, S.G.; Isaac, G.A. Quantification of the Effects of Shattering on Airborne Ice Particle Measurements. *J. Atmos. Ocean. Tech.* **2013**, *30*, 2527–2553. [CrossRef]
35. Baumgardner, D.; Spowart, M. Evaluation of the Forward Scattering Spectrometer Probe, Part III: Time Response and Laser Imhomogeneity Limitations. *J. Atmos. Ocean. Tech.* **1990**, *7*, 666–672. [CrossRef]
36. Brenguier, J.L.; Baumgardner, D.; Baker, B. A Review and Discussion of Processing Algorithms for FSSP Concentration Measurement. *J. Atmos. Ocean. Tech.* **1994**, *11*, 1409–1414. [CrossRef]
37. Brenguier, J.L.; Bourrianne, T.; Coelho, A.A.; Isbert, J.; Peytavi, R.; Trevarin, D.; Weschler, P. Improvements of Droplet Size Distribution Measurements with the Fast-FSSP (Forward Scattering Spectrometer Probe). *J. Atmos. Ocean. Tech.* **1998**, *15*, 1077–1090. [CrossRef]

38. Nagel, D.; Maixner, U.; Strapp, W.; Wasey, M. Advancements in Techniques for Calibration and Characterization of In Situ Optical Particle Measuring Probes, and Applications to the FSSP-100 Probe. *J. Atmos. Ocean. Tech.* **2007**, *24*, 745–760. [CrossRef]
39. Knollenberg, R.G. *Three New Instruments for Cloud Physics Measurements: The 2-D Spectrometer Probe, the Forward Scattering Spectrometer Probe, and the Active Scattering Aerosol Spectrometer*; Preprints; American Meteorological Society: Boston, MA, USA, 1976; pp. 554–561.
40. Knollenberg, R.G. Techniques for probing cloud microstructure. In *Clouds, Their Formation, Optical Properties and Effects*; Hobbs, P.V., Deepak, A., Eds.; Academic Press: Cambridge, MA, USA, 1981; pp. 15–91.
41. Glen, A.; Brooks, S.D. A new method for measuring optical scattering properties of atmospherically relevant dusts using the Cloud and Aerosol Spectrometer with Polarization (CASPOL). *Atmos. Chem. Phys.* **2013**, *13*, 1345–1356. [CrossRef]
42. Baumgardner, D.; Newton, R.; Krämer, M.; Meyer, J.R.; Beyer, A.; Wendisch, M.; Vochezer, P. The Cloud Particle Spectrometer with Polarization Detection (CPSPD): A next generation open-path cloud probe for distinguishing liquid cloud droplets from ice crystals. *Atmos. Res.* **2014**, *142*, 2–14. [CrossRef]
43. Vali, G.; Politovich, M.K.; Baumgardner, D.; Cooper, W.A. *Conduct of Cloud Spectra Measurements Scientific Report 1 to the Air Force Geophysical Laboratory*; Contract AFGL-TR-79-025; National Technical Information Service: Springfield, VA, USA, 1979; ADA081127.
44. Vali, G.; Politovich, M.K.; Baumgardner, D. *Conduct of Cloud Spectra Measurements, Final Report to Air Force Geophysics Laboratory*; Contract No. AFGL-TR-81-0122; National Technical Information Service: Springfield, VA, USA, 1981; ADA102944.
45. Mishchenko, M.I.; Travis, L.D.; Mackowski, D.W. T-matrix computations of light scattering by nonspherical particles: A review. *J. Quant. Spectrosc. Radiat. Transf.* **1996**, *55*, 535–575. [CrossRef]
46. Borrmann, S.; Beiping, L.; Mishchenko, M. Application of the T-matrix method to the measurement of aspherical (ellipsoidal) particles with forward scattering optical particle counters. *J. Aerosol Sci.* **2000**, *31*, 789–799. [CrossRef]
47. Meyer, J. *Ice Crystal Measurements with the New Particle Spectrometer NIXE-CAPS*; Forschungszentrum Julich GmbH; Institute for Energy and Climate Research: Jülich, Germany, 2012; 132p.
48. Schnaiter, M.; Buttner, S.; Mohler, O.; Skrotzki, J.; Vragel, M.; Wagner, R. Influence of particle size and shape on the backscattering linear depolarization ratio of small ice crystals—Cloud chamber measurements in the context of contrail and cirrus microphysics. *Atmos. Chem. Phys.* **2012**, *12*, 10465–10484. [CrossRef]
49. Hirst, E.; Kaye, P.H.; Greenway, R.S.; Field, P.; Johnson, D.W. Discrimination of micrometre-sized ice and super-cooled droplets in mixed-phase cloud. *Atmos. Environ.* **2001**, *35*, 33–47. [CrossRef]
50. Kaye, P.H.; Hirst, E.; Greenway, R.S.; Ulanowski, Z.; Hesse, E.; DeMott, P.; Saunders, C.; Connolly, P. Classifying atmospheric ice crystals by spatial light scattering. *Opt. Lett.* **2008**, *33*, 1545–1547. [CrossRef] [PubMed]
51. Lloyd, G.; Choularton, T.; Bower, K.; Crosier, J.; Gallagher, M.; Flynn, M.; Dorsey, J.; Liu, D.; Taylor, J.W.; Schlenczek, O.; et al. Small ice particles at slightly supercooled temperatures in tropical maritime convection. *Atmos. Chem. Phys.* **2020**, *20*, 3895–3904. [CrossRef]
52. Lawson, R.P.; Woods, S.; Jensen, E.; Erfani, E.; Gurganus, C.; Gallagher, M.; Connolly, P.; Whiteway, J.; Baran, A.J.; May, P.; et al. A review of ice particle shapes in cirrus formed in situ and anvils. *J. Geophys. Res. Atmos.* **2019**, *124*, 10049–10090. [CrossRef]
53. Abdelmonem, A.; Schnaiter, M.; Amsler, P.; Hesse, E.; Meyer, J.; Leisner, T. First correlated measurements of the shape and light scattering properties of cloud particles using the new Particle Habit Imaging and Polar Scattering (PHIPS) probe. *Atmos. Meas. Tech.* **2011**, *4*, 2125–2142. [CrossRef]
54. Gerber, H.; Arends, B.; Ackerman, A. New microphysics sensor for aircraft use. *Atmos. Res.* **1994**, *31*, 235–252. [CrossRef]
55. Gerber, H.; DeMott, P.J. Response of FSSP-100 and PVM-100A to Small Ice Crystals. *J. Atmos. Ocean. Tech.* **2014**, *31*, 2145–2155. [CrossRef]
56. Bohren, C.F.; Huffman, D.R. *Absorption and Scattering of Light by Small Particles*; John Wiley & Sons: New York, NY, USA, 1983.
57. Pinnick, R.G.; Auvermann, H.J. Response characteristics of Knollenberg light-scattering aerosol counters. *J. Aerosol Sci.* **1979**, *10*, 55–74. [CrossRef]
58. Gonser, S.G.; Klemm, O.; Griessbaum, F.; Chang, S.C.; Chu, H.S.; Hsia, Y.J. The relation between humidity and liquid water content in fog: An experimental approach. *Pure Appl. Geophys.* **2012**, *169*, 821–833. [CrossRef]
59. McFarquhar, G.M.; Um, J.; Jackson, R. Small Cloud Particle Shapes in Mixed-Phase Clouds. *J. Appl. Meteor.* **2013**, *52*, 1277–1293. [CrossRef]
60. McFarquhar, G.M.; Heymsfield, A.J.; Macke, A.; Iaquinta, J.; Aulenbach, S.M. Use of observed ice crystal sizes and shapes to calculate mean scattering properties and multi-spectral radiances: CEPEX April 4, 1993 case study. *J. Geophys. Res.* **1999**, *104*, 31763–31779. [CrossRef]
61. McFarquhar, G.M.; Yang, P.; Macke, A.; Baran, A.J. A New Parameterization of Single Scattering Solar Radiative Properties for Tropical Anvils Using Observed Ice Crystal Size and Shape Distributions. *J. Atmos. Sci.* **2002**, *59*, 2458–2478. [CrossRef]
62. Yang, P.; Baum, B.A.; Heymsfield, A.J.; Hu, Y.X.; Huang, H.L.; Tsay, S.C.; Ackerman, S. Single-scattering properties of droxtals. *J. Quant. Spectrosc. Radiat. Transf.* **2003**, *79–80*, 1159–1169. [CrossRef]
63. Nousiainen, T.; McFarquhar, G.M. Light Scattering by Quasi-Spherical Ice Crystals. *J. Atmos. Sci.* **2004**, *61*, 2229–2248. [CrossRef]
64. Pauling, L. The structure and entropy of ice and of other crystals with some randomness of atomic arrangement. *J. Am. Chem. Soc.* **1935**, *57*, 2680–2684. [CrossRef]

65. Stith, J.L.; Avallone, L.M.; Bansemer, A.; Basarab, B.; Dorsi, S.W.; Fuchs, B.; Lawson, R.P.; Rogers, D.C.; Rutledge, S.; Toohey, D.W. Ice particles in the upper anvil re- gions of midlatitude continental thunderstorms: The case for frozen-drop aggregates. *Atmos. Chem. Phys.* **2014**, *14*, 1973–1985. [CrossRef]
66. Um, J.; McFarquhar, G.M.; Stith, J.L.; Jung, C.H.; Lee, S.S.; Lee, J.Y.; Shin, Y.; Lee, Y.G.; Yang, Y.I.; Yum, S.S.; et al. Microphysical characteristics of frozen droplet aggregates from deep convective clouds. *Atmos. Chem. Phys.* **2018**, *18*, 16915–16930. [CrossRef]
67. Magee, N.; Boaggio, K.; Staskiewicz, S.; Lynn, A.; Zhao, X.; Tusay, N.; Schuh, T.; Bandamede, M.; Bancroft, L.; Connelly, D.; et al. Captured cirrus ice particles in high definition. *Atmos. Chem. Phys.* **2021**, *21*, 7171–7185. [CrossRef]
68. Järvinen, E.; Schnaiter, M.; Mioche, G.; Jourdan, O.; Shcherbakov, V.N.; Costa, A.; Afchine, A.; Krämer, M.; Heidelberg, F.; Jurkat, T.; et al. Quasi-Spherical Ice in Convective Clouds. *J. Atmos. Sci.* **2016**, *73*, 3885–3910. [CrossRef]
69. Um, J.; McFarquhar, G.M.; Hong, Y.P.; Lee, S.S.; Jung, C.H.; Lawson, R.P.; Mo, Q. Dimensions and aspect ratios of natural ice crystals. *Atmos. Chem. Phys.* **2015**, *15*, 3933–3956. [CrossRef]
70. Warren, S.G.; Brandt, R.E. Optical constants of ice from the ultraviolet to the microwave: A revised compilation. *J. Geophys. Res.* **2008**, *113*, D14220. [CrossRef]
71. Yurkin, M.A.; Hoekstra, A.G. The discrete-dipole-approximation code ADDA: Capabilities and known limitations. *J. Quant. Spectrosc. Radiat. Transf.* **2011**, *112*, 2234–2247. [CrossRef]
72. Bi, L.; Yang, P. Accurate simulation of the optical properties of atmospheric ice crystals with the invariant imbedding T-matrix method. *J. Quant. Spectrosc. Radiat. Transf.* **2014**, *138*, 17–35. [CrossRef]
73. Okada, Y. Efficient numerical orientation averaging of light scattering properties with a quasi-montecarlo method. *J. Quant. Spectrosc. Radiat. Transf.* **2008**, *109*, 1719–1742. [CrossRef]
74. Um, J.; McFarquhar, G.M. Optimal numerical methods for determining the orientation averages of single-scattering properties of atmospheric ice crystals. *J. Quant. Spectrosc. Radiat. Transf.* **2013**, *127*, 207–223. [CrossRef]
75. D'Alessandro, J.J.; McFarquhar, G.M.; Wu, W.; Stith, J.L.; Jensen, J.B.; Rauber, R.M. Characterizing the occurrence and spatial heterogeneity of liquid, ice, and mixed phase low-level clouds over the Southern Ocean using in situ observations acquired during SOCRATES. *J. Geophys. Res.* **2021**, *126*, e2020JD034482. [CrossRef]
76. Atlas, R.; Mohrmann, J.; Finlon, J.; Lu, J.; Hsiao, I.; Wood, R.; Diao, M. The University of Washington Ice–Liquid Discriminator (UWILD) improves single-particle phase classifications of hydrometeors within Southern Ocean clouds using machine learning. *Atmos. Meas. Tech.* **2021**, *14*, 7079–7101. [CrossRef]
77. Ulanowski, Z.; Hesse, E.; Kaye, P.H.; Baran, A.J. Light scattering by complex ice analogue crystal. *J. Quant. Spectro. Radiat. Transf.* **2006**, *100*, 382–392. [CrossRef]
78. Nousiainen, T.; Muñoz, O.; Lindqvist, H.; Mauno, P.; Videen, G. Light scattering by large Saharan dust particles: Comparison of modeling and experimental data for two samples. *J. Quant. Spectro. Radiat. Transf.* **2011**, *112*, 420–433. [CrossRef]
79. Morrison, H.; van Lier-Walqui, M.; Fridlind, A.M.; Grabowski, W.W.; Harrington, J.Y.; Hoose, C.; Korolev, A.; Kumjian, M.R.; Milbrandt, J.A.; Pawlowska, H.; et al. Confronting the challenge of modeling cloud and precipitation microphysics. *J. Adv. Model. Earth Syst.* **2020**, *12*, e2019MS001689. [CrossRef] [PubMed]